The Hippo pathway drives the cellular response to hydrostatic pressure

Title: The Hippo pathway drives the cellular response to hydrostatic pressure

Jiwon Park[1,2], Siyang JIA[1,2], Donald Salter[3], Pierre Bagnaninchi[2] and Carsten Gram Hansen[1,2,4]

[1]University of Edinburgh Centre for Inflammation Research, Institute for Regeneration and Repair, Queen's Medical Research Institute, Edinburgh bioQuarter, 47 Little France Crescent, Edinburgh EH16 4TJ, UK
[2] MRC Centre for Regenerative Medicine, Institute for Regeneration and Repair, University of Edinburgh, Edinburgh bioQuarter, 5 Little France Drive, Edinburgh EH16 4UU, UK
[3] Centre for Genomic & Experimental Medicine, MRC Institute of Genetics & Molecular Medicine, The University of Edinburgh, Western General Hospital
Crewe Road, Edinburgh, EH4 2XU
[4] Lead Contact

Abstract

Cells need to rapidly and precisely react to multiple mechanical and chemical stimuli in order to ensure precise context dependent responses. This requires dynamic cellular signalling events that ensure homeostasis and plasticity when needed. A less well understood process is cellular response to elevated interstitial fluid pressure, where the cell senses and responds to changes in extracellular hydrostatic pressure. Here using quantitative label-free digital holographic imaging, combined with genome editing, biochemistry and confocal imaging, we analyse the temporal cellular response to cyclic hydrostatic pressure. Upon elevated cyclic hydrostatic pressure, the cell responds by rapid, dramatic and reversible changes in cellular volume. We show that YAP and TAZ, the co-transcriptional regulators of the Hippo signalling pathway, control cell volume and that cells without YAP and TAZ have lower plasma membrane tension. We present direct evidence that YAP/TAZ drive the cellular response to hydrostatic pressure, a process that is at least partly mediated via clathrin-dependent endocytosis. Additionally, upon elevated oscillating hydrostatic pressure, YAP and TAZ are activated and induce TEAD mediated transcription and expression of cellular components involved in dynamic regulation of cell volume and extracellular matrix. This cellular response confers a feedback loop that allows the cell to robustly respond to changes in interstitial fluid pressure.

Keywords:

YAP/TAZ, endocytosis, membrane tension, cell volume, holographic imaging

Introduction:

Cells constantly need to sense and dynamically integrate multiple chemical and mechanical stimuli within the cellular microenvironment (Cadart, 2019b; Collinet, 2021; Hansen *et al*, 2015a; Vining & Mooney, 2017). Physical cues in the cellular niche are critical mediators of context dependent cellular regulation and responses (Cadart, 2019b; Collinet, 2021; Hansen *et al.*, 2015a; Vining & Mooney, 2017). Consequently, in-depth understanding of how cells respond to these distinct forces are of major interest. These fundamental responses modulate central cellular processes, such as metabolic adaptation, differentiation, proliferation, cellular migration and cell size, and thereby ultimately define cell identity (Cadart, 2019b; Collinet, 2021; Hansen *et al.*, 2015a; Vining & Mooney, 2017). A less well understood cellular process is the ability to precisely and dynamically respond to changes in

interstitial fluid pressure (IFP). This pressure is distinct from other types of cellular mechanical stimuli, as IFP is isotropic and affects the thermodynamics of the cellular environment without applying a vector force (Heldin *et al*, 2004; Myers *et al*, 2007). Consequently, fluid pressure is fundamentally different to other mechanical stresses. IFP oscillates almost in phase with arterial pressure (Myers *et al.*, 2007). IFP is of particular importance during development (Chan & Hiiragi, 2020; Mirra *et al*, 2019; Stewart *et al*, 2011; Teng & Engler, 2019), but also during pathophysiological processes, such as inflammation, oedema and in solid tumours (Heldin *et al.*, 2004; Stewart *et al.*, 2011; Teng & Engler, 2019; Wiig & Swartz, 2012). Tumours with elevated IFP facilitate the migration of cancer cells from the tumour into the tissue and correlate with poor prognosis (Heldin *et al.*, 2004; Northcott *et al*, 2018). Various factors may contribute to elevated IFP in solid tumours, including blood-vessel leakiness, contraction mediated by stromal fibroblasts and overall changes to the interstitial matrix composition, as well as from lymph vessel abnormalities (Heldin *et al.*, 2004; Myers *et al.*, 2007; Swartz & Lund, 2012; Wiig & Swartz, 2012).

The Hippo pathway, through regulating its transcriptional co-activators YAP and TAZ, controls development and facilitates regenerative processes, and if the pathway is not tightly regulated causes cancer (Davis & Tapon, 2019; Fulford *et al*, 2018; Moroishi *et al*, 2015a; Rognoni & Walko, 2019; Salem & Hansen, 2019; Thompson, 2020; Zanconato *et al*, 2019). The Hippo pathway contains an upstream serine/threonine kinase module and a downstream transcriptional effector module, consisting of YAP and TAZ (encoded respectively by *YAP1* and *WWTR1)* and their cognate transcription factors (Fulford *et al.*, 2018; Hansen *et al.*, 2015a). YAP/TAZ are regulated by LATS1/2 mediated inhibitory phosphorylation on five (YAP) or four (TAZ) serine residues (Huang *et al*, 2005; Liu *et al*, 2010; Zhao *et al*, 2007). Upon relief from this inhibitory phosphorylation, YAP and TAZ localise to the nucleus to exert their co-transcriptional activity (Huang *et al.*, 2005; Liu *et al.*, 2010; Zhao *et al.*, 2007). In solid tumours, high YAP/TAZ activity in general increase the risk of metastasis (Lamar *et al*, 2012; Steinhardt *et al*, 2008), impede cancer treatment and confer poor prognosis (Moroishi *et al.*, 2015a; Rognoni & Walko, 2019; Salem & Hansen, 2019; Thompson, 2020; Zanconato *et al.*, 2019). However, distinct core Hippo pathway components are mutated only in a subset of cancers, and the underlying reasons as to why YAP/TAZ are predominantly nuclear in solid tumours are not fully understood (Fulford *et al.*, 2018; Moroishi *et al.*, 2015a; Rognoni & Walko, 2019; Salem & Hansen, 2019; Thompson, 2020; Zanconato *et al.*, 2019). The Hippo pathway is a transducer of physical stimuli in the microenvironment and a nexus for cellular signalling (Hansen *et al.*, 2015a; Rausch & Hansen, 2020). The Hippo pathway is linked to cellular responses to extracellular matrix (ECM) stiffness (Bertero *et al*, 2016; Dupont *et al*, 2011; Liu *et al*, 2015; Meng *et al*, 2018), shear stress (Lee *et al*, 2017; Nakajima *et al*, 2017; Rausch *et al*, 2019; Wang *et al*, 2016) and osmotic pressure (Hong *et al*, 2017; Meng *et al.*, 2018). Importantly, the pathway's role in cellular response to elevated hydrostatic pressure has so far been unexplored. As the Hippo pathway is a mechanotransductive pathway, we sought to establish if the Hippo pathway is a mediator of the cellular response to interstitial fluid pressure. We took advantage of a panel of isogenic genome-edited cells (Hansen *et al*, 2015b; Lin *et al*, 2017; Meng *et al*, 2015; Rausch *et al.*, 2019) where core

components of the pathway have been deleted. This isogenic platform allows us to directly evaluate the impact components within the Hippo pathway has on fundamental cellular functions. We here provide evidence that changes in hydrostatic pressure is sensed at the plasma membrane via regulation of clathrin-mediated endocytosis, which is transduced to the core Hippo pathway kinase module and initiates downstream YAP/TAZ-TEAD dependent cellular effects. This highlights how hydrostatic forces, plasma membrane tension and dynamics, stimulate intracellular signals and regulate cell functions.

Results:

Oscillating hydrostatic pressure activates YAP/TAZ

Initially we examined if the Hippo pathway is responsive to hydrostatic pressure and examined 200 mbar, readily within the pathophysiological range of cellular interstitial fluid pressures (DuFort, 2016; Heldin *et al.*, 2004). HEK293A cells were cultured with or without cyclic hydrostatic pressure for two hours, whereafter lysates were prepared and analysed by PhosTag gels (Fig 1A and 1B). YAP and YAZ are inhibited by LATS1/2-mediated phosphorylation on multiple sites (Meng *et al.*, 2015; Mo *et al*, 2012; Moroishi *et al*, 2015b; Park *et al*, 2015; Yu *et al*, 2012; Zhao *et al.*, 2007). Consequently, the PhosTag technique allows for determination of YAP and TAZ phosphorylation levels, and thereby activation status (Meng *et al.*, 2015; Mo *et al.*, 2012; Moroishi *et al.*, 2015b; Park *et al.*, 2015; Yu *et al.*, 2012; Zhao *et al.*, 2007). A clear down shift (dephosphorylation), and therefore activation of YAP (Fig 1A) and TAZ (Fig 1B) are observed in cells experiencing cyclic hydrostatic pressure. To further confirm that the observed changes in dephosphorylation levels cause an increase in YAP/TAZ activity levels, we analysed the same lysates by conventional Western blots (Fig 1C). Increased levels of YAP and TAZ were evident in these experiments consistent with elevated YAP and TAZ activity. Using phospho-specific YAP antibodies raised against S127, a major LATS site (Zhao *et al.*, 2007), as well as using antibodies that exclusively recognises S127 when YAP is not phosphorylated on this site (Si *et al*, 2017) (Fig 1C), confirmed results obtained by PhosTag gels. Protein levels of two well established YAP/TAZ targets, CTGF (*CCN2*) and CYR61 (*CCN1*), are likewise increased upon cyclic hydrostatic pressure (Fig 1C). These data show that YAP/TAZ are dephosphorylated on inhibitory phosphorylation sites upon increased cyclic pressure, and that protein levels of well-established YAP/TAZ encoded target genes are increased upon oscillating hydrostatic pressure (Fig 1C). We next examined if this cellular response is conserved in additional cell types. As elevated IFP is well established in primary bone cancer (Ariffin *et al*, 2014; Matsubara *et al*, 2013; Nathan *et al*, 2005; Nathan *et al*, 2008), we examined the osteosarcoma derived cell line 143B. Indeed in 143B cells, as in HEK293A cells, YAP becomes dephosphorylated upon oscillating hydrostatic pressure (Fig 1D, E). Furthermore, total 143B cellular levels of YAP and TAZ, likely due to increased stability of unphosphorylated protein (Zhao *et al*, 2010), as well as CTGF and CYR61 are elevated upon cyclic hydrostatic pressure (Fig 1E) mirroring the effect observed in HEK293A cells. We next examined cells experiencing comparable levels of static hydrostatic pressure and observed no YAP

activation (EV 1A), which highlights that cells sense and respond to dynamic changes. A major point of YAP/TAZ regulation is via nuclear/cytoplasmic shuttling, as increased LATS1/2 phosphorylation renders YAP and TAZ cytoplasmic (Meng *et al.*, 2015; Mo *et al.*, 2012; Moroishi *et al.*, 2015b; Park *et al.*, 2015; Yu *et al.*, 2012; Zhao *et al.*, 2010; Zhao *et al*, 2012). Therefore, we next examined the subcellular localisation of YAP in HEK293A cells experiencing cyclic hydrostatic pressure. As predicted from our immunoblots (Fig 1A-C), YAP translocate to the nucleus upon oscillating hydrostatic pressure (Fig 1F). In parallel experiments, we analysed YAP localisation in 143B cells. As in HEK293A cells, YAP translocate to the nucleus upon elevated hydrostatic pressure (Fig 1G). We next took advantage of genome-edited YAP/TAZ deficient cells (Hansen *et al.*, 2015b) (Fig 1H) to establish if YAP/TAZ drive the transcriptional regulation of the cellular response to hydrostatic pressure. We analysed the levels of the well-established YAP/TAZ target genes *CYR61* and *CTGF* in cells challenged with cyclic hydrostatic pressure and compared those to cells at steady state. A clear induction of *CYR61* and *CTGF* encoding extracellular matrix proteins is evident in cells experiencing oscillating fluid pressure (Fig 1I). Comparing this effect to the cellular response in YAP/TAZ knockouts (Fig 1H) allowed us to establish that this cellular response to hydrostatic pressure is dependent on YAP/TAZ (Fig 1I, J). These data combined confirms that YAP/TAZ are activated upon oscillating hydrostatic pressure.

YAP/TAZ regulate cell volume

To establish the macroscopic cellular response to hydrostatic pressure, we took advantage of live cell digital holographic imaging (DHM), a technique that allows for quantitative label free cellular imaging with single cell resolution (Marquet P, 2005). Initially, we examined the cellular volume across genotypes (Fig 2A-D) derived from the optical volume under the assumptions described in the methods. The average cellular volume of two independent YAP/TAZ knock out clones (Hansen *et al.*, 2015b) are 1,154 $\pm$348μm^3 (mean $\pm$SD) (Y/T DKO#1) and 1,273 $\pm$ 352μm^3 (mean $\pm$SD) (Y/T DKO#2) whereas the average cell volume of wild type cells are 1,532 $\pm$434μm^3 (mean $\pm$SD). Y/T DKO cells are therefore ~16-25% smaller than wild type cells (Fig 2A). These data confirm recent reports highlighting that YAP/TAZ regulate cell size via signalling to mTORC1, and through other less defined mechanisms (Hansen *et al.*, 2015b; Mugahid *et al*, 2020; Perez-Gonzalez *et al*, 2019; Plouffe *et al*, 2018). LATS1/2 directly phosphorylate and thereby inhibit YAP/TAZ and are the major cellular regulators of YAP/TAZ (Meng *et al.*, 2015; Mo *et al.*, 2012; Moroishi *et al.*, 2015b; Park *et al.*, 2015; Yu *et al.*, 2012; Zhao *et al.*, 2010; Zhao *et al.*, 2012). YAP/TAZ are consequently nuclear and constitutively activated in LATS1/2 DKO cells (Meng *et al.*, 2015; Park *et al.*, 2015). Consistent with YAP/TAZ DKO cells being smaller, the average cell volume of LATS1/2 DKO with hyperactive YAP/TAZ are 1,603$\pm$ 473μm^3 (mean $\pm$SD) (LATS1/2 DKO#1) and 1,731$\pm$ 526μm^3 (mean $\pm$SD) (LATS1/2 DKO#2). The larger cell volume of LATS1/2 DKO cells compared to WT (Fig 2B, EV 1B) confirms previous observations (Hansen *et al.*, 2015b).

These data firmly establish our ability to precisely measure the cellular volume change associated with modification of the Hippo pathway. Using this approach, together with the isogenic Hippo pathway component knockout models (Hansen *et al.*, 2015b; Lin *et al.*, 2017; Meng *et al.*, 2015; Park *et al.*, 2015), allow us to delineate

the potential role of discrete Hippo pathway components on cell volume.
MST1/2 phosphorylate and activate LATS1/2 (Hansen *et al.*, 2015a; Moroishi *et al.*, 2015a). To gain mechanistic insights into cellular volume regulation, we went on to determine the cell volume of cells without the Hippo kinases (MST1/2) (Huang *et al.*, 2005; Meng *et al.*, 2015). MST1/2 DKO cells are of similar size as WT cells (Fig 2C). MST1/2 DKO cells therefore do not phenocopy LATS1/2 DKO cells in respect to cellular volume. This is likely due to further regulation of LATS1/2 by MST1/2 compensating LATS1/2 activating kinases (Li *et al*, 2014b; Li *et al*, 2018; Meng *et al.*, 2015; Rausch & Hansen, 2020). We also examined the cellular volume of cells devoid of NF2. NF2, also known as MERLIN, is a tumour suppressor and functions as an upstream positive regulator of the Hippo pathway kinases (Meng *et al.*, 2015; Zhang *et al*, 2010). NF2 is the most commonly mutated Hippo pathway component in cancers, and NF2 loss of function mutations are especially prevalent in pleural mesothelioma (Moroishi *et al.*, 2015a; Petrilli & Fernandez-Valle, 2016). YAP/TAZ are hyperactive in cells without NF2 (Moroishi *et al.*, 2015a; Petrilli & Fernandez-Valle, 2016). NF2 KO cells are 25.8% larger than WT cells (1728± 439μm^3 (mean ±SD)) (Fig 2D, EV 1C) and therefore phenocopy LATS1/2 DKO cells. As the co-transcriptional activators YAP/TAZ frequently regulate gene expression via binding to the TEAD transcription factors (Hansen *et al.*, 2015b; Lamar *et al.*, 2012; Li *et al*, 2010; Park *et al.*, 2015; Rausch *et al.*, 2019; Vassilev *et al*, 2001; Zhang *et al*, 2009; Zhao *et al*, 2008), we examined the cellular volume in cells without TEADs (these cells express low levels of TEAD3 (Lin *et al.*, 2017)). Analysing two independent TEAD KO clones revealed that TEADs do not dictate the steady state cellular volume (Fig 2E, EV 1D), and consequently, the role of YAP/TAZ in regulating the cellular volume at steady state takes at least partly place via additional transcription factors (Hansen *et al.*, 2015a).

Cells respond to oscillating hydrostatic pressure by YAP/TAZ-TEAD dependent rapid volume changes

As the cellular consequences of increased interstitial fluid pressure are not well established (Heldin *et al.*, 2004; Li *et al*, 2020; Myers *et al.*, 2007), we sought to determine if the force exerted by hydrostatic pressure regulates cell size. To this end, we established a workflow that allows us to analyse the dynamic cellular response to elevated hydrostatic pressure in real time with a temporal resolution of seconds. In our system, the hydrostatic pressure is controlled by a microfluidic pump coupled to closed cell culture chambers, where cells are imaged using digital holographic microscopy (Marquet P, 2005). We are consequently able to dictate the precise and temporal hydrostatic pressure experienced by cells, driven by the extra- and intracellular pressure differences, in a physiologically relevant manner while imaging the cells without labelling and at single cell resolution.
When the fluid pressure is modulated with a peak-to-peak pressure of 100 mbar and a 10 second cycle, a clear corresponding cyclic change in volume for the WT cells (6.79 ± 2.89% (mean ±SD) (Fig 2F-H) is observed. In contrast YAP/TAZ DKO cells exhibited a substantially smaller periodic volume change (Y/T DKO#1 5.03 ± 1.88% (mean ±SD), Y/T DKO#2 4.42 ± 2.02% (mean ± SD)) (Fig 2G, H). This YAP and TAZ dependence on the cellular response to hydrostatic pressure is conserved in 143B cells (EV 1E, F). In order to further characterize how cells depleted of YAP/TAZ

differ to WT cells, we took advantage of the membrane tension probe “Flipper-TR” (Colom *et al*, 2018; Riggi *et al*, 2018). The Flipper probe inserts into the lipid bilayer and its mechanophore composition is altered depending on the organization of lipid bilayers. The conformational changes of the probe induced by membrane tension alter the excitation maxima and fluorescence lifetime, which can be quantified using fluorescence lifetime imaging microscopy (FLIM) (Colom *et al.*, 2018; Riggi *et al.*, 2018). Using this probe and comparing WT to Y/T DKO HEK293A cells a substantial decrease in membrane tension is observed upon deletion of YAP/TAZ (Fig 1I, J). This highlights a distinct, so far unrecognised, YAP/TAZ dependent difference on the physical properties of the plasma membrane.

To further investigate that the effect observed upon hydrostatic pressure in the knock out clones is due to lack of YAP/TAZ, we reintroduced YAP into YAP/TAZ DKO HEK293A cells (Fig 2K, L). YAP/TAZ do not bind DNA directly but function as transcriptional co-activators through diverse sets of transcription factors (Hansen *et al.*, 2015a), the TEAD family being the most prominent mediator of YAP/TAZ activity (Hansen *et al.*, 2015b; Huh *et al*, 2019; Lamar *et al.*, 2012; Li *et al.*, 2010; Ota & Sasaki, 2008; Rausch *et al.*, 2019; Vassilev *et al.*, 2001; Zhao *et al.*, 2008). We sought to establish if the observed YAP/TAZ contingent cellular response also depend on TEADs and generated separate stable cell lines of MYC-tagged WT YAP and of a TEAD binding deficient YAP (S94A) (Li *et al.*, 2010; Zhao *et al.*, 2008). Cell populations were >95% positive for YAP (Fig 2K), and cells re-expressing WT YAP, but not S94A YAP rescue CYR61 expression functionally validating these cell lines (Fig 2L). Introduction of exogenous wild type YAP into YAP/TAZ knock out cells, but not S94A YAP rescue the cellular response to cyclic fluid pressure (Fig 2M). Introduction of exogenous TAZ into YAP/TAZ knock out cells likewise rescued the cellular response to cyclic fluid pressure (EV 1H-J), highlighting that YAP or TAZ driven TEAD activation is sufficient to drive the cellular response to hydrostatic pressure.

We in a complimentary approach took advantage of TEAD knockout HEK293A cells (EV 1D) (Lin *et al.*, 2017). We hypothesised that if YAP/TAZ works via TEADs to dictate cellular volume via hydrostatic pressure, TEAD deficient cells would phenocopy YAP/TAZ knock out cells. Consistent with this, TEAD deficient cells closely mirror YAP/TAZ knock out cells regarding their cellular response to cyclic fluid pressure (Fig 2N). Consequently, we conclude that the cellular response to hydrostatic pressure is dependent on YAP/TAZ-TEAD activity. Using our robust cell volume change assay as read out for cellular response to fluid pressure, we next analysed LATS1/2 DKO, MST1/2 DKO and NF2 KO cells. Cells with these genotypes have varying degrees of hyperactive YAP/TAZ (Hansen *et al.*, 2015b; Meng *et al.*, 2015; Meng *et al.*, 2018), but have similar response to hydrostatic pressure (EV 2A-C) highlighting that increased YAP/TAZ levels above WT levels do not change the cell volume response to fluid pressure. We next sought to establish the longer-term impact on cells upon changes in hydrostatic pressure. We initially measured by DHM the steady state cell volume and compared this to the steady state volume of cells that had undergone two hours of oscillating 100 mbar hydrostatic pressure (with pre-conditioning). Both WT and YAP/TAZ do not change their cellular volume after hydrostatic pressure, regardless of prior exposure to hydrostatic pressure (Fig 2O). To obtain insights into if cells adapt their dynamic cell volume response to oscillating hydrostatic pressure, we in similar experiments as above compared the average

change in cell volume between cells without any previous exposure to hydrostatic pressure to cells with prior exposure to oscillating hydrostatic pressure (Fig 2P). Cells with prior exposure to oscillating hydrostatic pressure adapt to this by lowering their volume changes, but interestingly this mechanical memory is lost in Y/T KO cells (Fig 2P). In order to establish transcriptional regulation of surface molecules for potential long-term adaption of the cellular response to hydrostatic pressure, we undertook a candidate approach of genes previously shown to be involved in cell volume regulation. We analysed WT cells after 4 hours of oscillating hydrostatic pressure stimulation and analysed gene expression and identified a range of specific genes involved in dynamic cell volume regulation that is robustly induced, including *LRRC8A,B,C and E* (Kefauver *et al*, 2018; Qiu *et al*, 2014; Voss *et al*, 2014) encoding components of the heteromeric Volume Regulated Anion Channel (VRAC), as well as genes encoding homotetrameric aquaporins (*AQP6* and *11*) (Yasui *et al*, 1999), the nonselective cation channel transient receptor potential vanilloid 1 (*TRPV1*) (Liao *et al*, 2013) and the swelling-activated TRPM7 cation channels (Numata *et al*, 2021; Schmitz *et al*, 2003), but not other mechanotransductive active plasma membrane components, such as the mechanosensitive ion channel *PIEZO1 (Coste et al, 2010; Li et al, 2014a)* and the essential caveolae gene *CAV1* (Hansen & Nichols, 2010; Rausch *et al.*, 2019; Rausch & Hansen, 2020) (EV 1K). In order to examine the role of YAP/TAZ in this transcriptional regulation, we analysed the induction of these specific gene-sets in each of the two Y/T DKO clones, and compared this to that of WT cells (EV 1L, M). There is a marked decrease in the induction of the fold induction of these genes in Y/T DKO cells (EV 1L, M). This suggests that the hydrostatic pressure mediated transcriptional induction of specific gene-sets is YAP/TAZ dependent, and highlights that YAP/TAZ likely also regulate long-term cellular adaption to hydrostatic pressure.

Actin cytoskeletal regulation of the cellular volume

The actin cytoskeleton and cortex are regulators and mediators of cellular deformations (Chugh *et al*, 2017; Stewart *et al.*, 2011; van Helvert *et al*, 2018). The Hippo pathway is a transducer of mechanical cues and is regulated via actin cytoskeletal changes (Dupont *et al.*, 2011; Li *et al.*, 2018; Meng *et al.*, 2018; Sansores-Garcia *et al*, 2011; Yu *et al.*, 2012; Zhao *et al.*, 2012), including via transcriptional regulation of cytoskeletal components and modifiers and thereby controling the dynamics of the actomyosin network (Kim *et al*, 2017; Lucas *et al*, 2013; Mason *et al*, 2019; Nardone *et al*, 2017; Porazinski *et al*, 2015; Qiao *et al*, 2017; Zhao *et al.*, 2008).

To gain further mechanistic insights into the cellular response to hydrostatic pressure, we set out to analyse the impact of disrupting the cytoskeleton using Cytochalasin D (CytD) and sought to establish if the cellular volume changes upon actin disruption. CytD lowered the overall cell volume across genotypes (Fig 3A and B). This prompted us to examine if actin disruption changes the cellular response to cyclic fluid pressure. Initially, we examined by immunofluorescence that the established actin disruptors Latrunculin B (LatB) and CytD work across the genotypes in a similar manner (Fig 3C). This was indeed the case, as the organization of phalloidin labelled actin filaments is severely disrupted in WT, Y/T DKO and LATS1/2 DKO cells (Fig 3C). We next confirmed that these chemicals

inhibit YAP by treating cells with either LatB or CytD and examining the cell lysates on PhosTag gels followed by immunoblots. As expected (Yu *et al.*, 2012; Zhao *et al.*, 2012), we noticed an upshift of YAP upon LatB and CytD treatment (EV 2D). To establish if the difference in cell volume, we observed across genotypes (EV 2D-F) is conserved upon actin disruption, we compared the observed change in cellular volume to the overall effect CytD have on WT cells (Fig 3A and B). We find that the divergent cellular volume across genotypes is not dependent on a functional actin cytoskeleton (Fig 3A-C). Consequently, additional factors such as differentially expressed cytoskeletal factors, changes within the plasma membrane or cellular volume sensing (EV 1L,M) operating independently of the actin cytoskeleton are likely factors dictating this difference.

Actin cytoskeletal dependence on the cellular response to oscillating fluid pressure

We next set out to establish if the actin cytoskeleton mediates the cellular response to fluid pressure via the Hippo pathway. First, we analysed WT cells treated with CytD or LatB under cyclic fluid pressure, which revealed that the cellular response to hydrostatic pressure in WT cells is strongly dependent on the actin cytoskeleton (Fig 3D, F). This actin dependence is conserved in Y/T DKO cells in contrast to LATS1/2 DKO cells. Cell volume response to hydrostatic pressure in LATS1/2 DKO cells are insensitive to LatB and CytD. This highlights that LATS1/2 deficient cells have additional mechanisms to ensure cellular response to hydrostatic pressure (Fig 3D-G). Taken together, our data reveal that differences in cellular volume upon alterations in fluid pressure across genotypes are not solely due to genotype specific alterations causing modifications to the actin cytoskeleton. Consequently, additional factors operating independently of the actin cytoskeleton dictates this difference.

Microtubule regulation of the cellular volume and response to oscillating fluid pressure

Microtubules in some instances, like actin, function as mechanotransducers (Rafiq *et al*, 2019; Salmon, 1975). We therefore sought to establish the role of microtubules in the cellular response to cyclic hydrostatic pressure by treating cells with the microtubule depolymerisation drug nocodazole (NCD). Initially, we established by immunofluorescence that the cellular microtubules are severely disrupted upon short-term (10 min) NCD treatment across the genotypes (Fig 4A) and confirmed that the actin cytoskeleton is comparable across genotypes upon short-term microtubule depolymerisation (Fig 4B). When comparing the cellular effect upon microtubule depolymerisation, the steady state cell volume across genotypes is conserved (Fig 4C), as well as a preserved cellular response towards hydrostatic pressure in Y/T DKO cells but not in LATS1/2 DKO cells. LATS1/2 DKO cells with disrupted microtubules (Fig 4A) respond to cyclic fluid pressure by an increased cellular volume change (Fig 4D). This prompted us to analyse the cellular response to hydrostatic pressure of combined actin cytoskeleton and microtubules disruption in WT and LATS1/2 DKO cells (Fig 4E). Combined NCD and CytD treated WT cells experiencing cyclic fluid pressure phenocopied CytD treated WT cells (Fig 3D, 4E). NCD and CytD treatment of LATS1/2 DKO cells abolished the increased volume change observed in microtubule disrupted LATS1/2 DKO cells (Fig 4D, E), which highlights that this aspect is actin dependent. As mTORC1 is a major regulator of cell size (Liu & Sabatini, 2020), we asked if mTORC1 inhibition had consequences on

cellular response to cyclic hydrostatic pressure. Medium-term (40 minutes) mTORC1 inhibition using two distinct and widely used mTORC1 inhibitors, namely the ATP-competitive inhibitor Torin and the macrolide Rapamycin (Liu & Sabatini, 2020), do not change the cellular volume or cellular response to hydrostatic pressure (EV 3A-C). Overall, we conclude that the actin cytoskeleton mediates the cellular response to hydrostatic pressure.

Clathrin dependent endocytosis mediate the cellular response to hydrostatic pressure

As the cellular volume change is reversible and fast (within seconds) (Fig 2G) the surface area of the plasma membrane needs to dynamically and rapidly change. Taken a simplified view that the plasma membrane does not change area directly by stretching and that the cell is spherical, this 6.7% increase (Fig 2 A-F) in cellular volume ($(V_1-V_o)/V_o$) would equate to a change of plasma surface of 4.42% ($S_1-S_o)/S_o=((V_1^{2/3}-V_o^{2/3})/V_o^{2/3})$). We and others recently discovered that caveolae, 60-100nm invaginations of the plasma membrane composed of the structural caveolae proteins CAVEOLINs and CAVINs (Hansen & Nichols, 2010) mediate cellular YAP/TAZ shear stress (Rausch *et al.*, 2019) and substrate stiffness (Moreno-Vicente *et al*, 2019) responses (Rausch & Hansen, 2020). We therefore examined if the cellular response to hydrostatic pressure is mediated via caveolae. However, cells devoid of the essential caveolar protein, CAVEOLIN1 are comparable to WT cells in their response to fluid pressure (EV 3D-H). An alternative way for the cell surface to undergo reversible change is through altering the rates of endocytosis (Kaksonen & Roux, 2018). Several types of endocytosis exist including macropinocytosis, caveolae mediated endocytosis, clathrin dependent endocytosis (CDE) and additional less well defined clathrin independent internalization processes (Hansen & Nichols, 2009; Kaksonen & Roux, 2018). Of these, CDE is the best characterised. In CDE, a range of adaptor proteins, including AP2, actin filaments and the ANTH domain containing protein AP180 are recruited to the plasma membrane and cause formation of clathrin coats (Pearse, 1976) in a precise and temporal manner (Akamatsu *et al*, 2020; Ford *et al*, 2001; Taylor *et al*, 2011; Yoshida *et al*, 2018), where after the coated vesicles with internalized cargo are pinched off by the recruitment of the large GTPase Dynamin (Akamatsu *et al.*, 2020; Ford *et al.*, 2001; Taylor *et al.*, 2011; Yoshida *et al.*, 2018). Importantly, CDE is mechanosensitive (Akamatsu *et al.*, 2020; Baschieri *et al*, 2020; Boulant *et al*, 2011; Ferguson *et al*, 2017; Malinverno *et al*, 2017; Saleem *et al*, 2015) and in non-specialized cells account for upwards of 95% internalisation of the plasma membrane (Bitsikas *et al*, 2014). CDE therefore represents the major route for internalization of the plasma membrane and the process is an attractive pathway that could confer the change of cell surface plasma membrane necessary for changing the cellular volume. To test this hypothesis, we used fluorescently labelled transferrin (Trf) that binds to the transferrin receptor and is internalised exclusively via clathrin-mediated endocytosis (Bitsikas *et al.*, 2014; Ford *et al.*, 2001; Taylor *et al.*, 2011; Yoshida *et al.*, 2018). Using an established internalisation assay, where surface bound Trf is stripped off the plasma membrane, we compared the internalisation of Trf across WT, Y/T DKO, and LATS1/2 DKO cells at steady state (Fig 5A and B). The internalisation rate of Trf and thereby CDE at steady state in Y/T DKO is comparable to WT cells, whereas LATS1/2 DKO cells internalize Trf faster (Fig 5A and B). We next examined if

hydrostatic pressure influences CDE under the same assay conditions used previously. We noticed a robust upregulation of Trf uptake upon cyclic hydrostatic pressure in both HEK293A and 143B cells (Fig 5A, B and EV 4A, B). This effect is conserved in LATS1/2 DKO cells, but not in cells without YAP/TAZ (Fig 5A, B). Oscillating hydrostatic pressure therefore increases the rate of CDE in a YAP/TAZ dependent manner. The increased hydrostatic pressure mediated internalisation rate is specific to CDE, as rates of fluid phase internalisation as measured by uptake of fluorescently labelled dextran does not increase (EV 4C-H). To firmly establish the role of CDE in this process, we took advantage of a dominant negative CDE construct. This construct encodes the C terminus of the adaptor protein 180 (AP180C), and blocks clathrin-mediated endocytosis (Ford *et al.*, 2001). We initially expressed AP180C in WT and Y/T DKO cells to establish that AP180C function is YAP/TAZ independent. A robust decrease in Trf uptake in all AP180C expressing cells is, as expected, evident (Fig 5C and D). We next sought to analyse the effect of AP180C expression on YAP. We co-labelled WT or LATS1/2 DKO cells expressing either vector or AP180C and analysed these by confocal microscopy. YAP localised predominantly in the cytoplasm in WT AP180C expressing cells, an effect not observed in LATS1/2 DKO cells (Fig 5E and F). YAP therefore gets inactivated upon CDE inhibition in a LATS1/2 dependent manner. Our immunofluorescence-based assay also allowed us to establish that our transfection efficiency is >80%, which prompted us to analyse pools of cells expressing AP180C using DHM at the single cell level. In WT cells expressing AP180C, the cellular volume change upon cyclic fluid pressure is diminished to levels comparable to Y/T DKO cells (Fig 5G, EV 2I), whereas AP180C had no effect on the cellular response to hydrostatic pressure in LATS1/2 DKO and Y/T DKO cells (Fig 5G, EV 2I). LATS1/2 are activated by either MST1/2 (the *hpo* kinases), or by the MAP4K family members as alternative direct LATS1/2 activating kinases (Li *et al.*, 2014b; Meng *et al.*, 2015; Zheng *et al*, 2015). In order to define which parts of the upstream kinase module are critical for sensing and integrating the clathrin-dependent endocytic cellular response to hydrostatic pressure to the Hippo pathway, we transfected vector control or AP180C into an expanded range of isogenic cell lines (Hansen *et al.*, 2015b; Meng *et al.*, 2015) including WT, LATS1/2 DKO, MST1/2 DKO, MAP4K4/6/7 KO, MST1/2-MAP4K4/6/7 KO, and MST1/2-MAP4K1/2/3/4/6/7 KO cells. These transfected cells were stimulated with oscillating hydrostatic pressure and changes in YAP phosphorylation levels were analysed by PhosTag. A clear upshift (increased YAP phosphorylation) is observed in WT and MAP4K4/6/7 KO cells, but not in LATS1/2 DKO, MST1/2 DKO, MST1/2-MAP4K4/6/7 KO or MST1/2-MAP4K1/2/3/4/6/7 KO cells (EV 5A-F). These findings suggests that YAP is inhibited and cytosolic in AP180C MAP4K4/6/7 KO, but not in MST DKO cells stimulated with oscillating hydrostatic pressure. In order to confirm this, in complimentary experiments, we compared changes in the nuclear localisation of YAP between AP180C transfection positive and transfection negative cells within the same field of view upon stimulation with cyclic hydrostatic pressure. A marked decrease in YAP nuclear localisation was observed in MAP4K4/6/7 KO cells, but not in MST1/2 KO cells (EV 5G,H), which highlights the role of MST1/2 in the integration of CDE with downstream cellular effects induced by hydrostatic pressure. We conclude that CDE is regulated by hydrostatic

pressure in a YAP/TAZ dependent manner and function as a mediator of the cellular response to hydrostatic pressure.

Cell volume regulation at steady state and upon hydrostatic pressure differ in some aspects, but both regulations centres on the Hippo pathway transcriptional mediators YAP/TAZ. We here establish that YAP and TAZ regulate plasma membrane tension, and that YAP/TAZ are critical regulators of cell volume, and that hydrostatic pressure and CDE are additional factors that dynamically dictates this fundamental cell volume regulatory process. This intricate feedback underlies the cellular response to hydrostatic pressure.

Discussion

Our studies reveal through quantitative single cell measurements that oscillating fluid pressure induces fast cell-size fluctuations dependent on YAP/TAZ. Cells devoid of YAP/TAZ are smaller and have a lower membrane tension and are therefore less adaptable to rapid cell shape changes. We show that this dynamic cellular response is contingent on both the cytoskeleton and clathrin dependent endocytosis. YAP/TAZ are dephosphorylated and consequently activated upon elevated cyclic fluid pressure. This activation drives a transcriptional response, including of the matricellular proteins CYR61 and CTGF. CYR61 and CTGF have established roles in development, as well as in pro-tumorigenic and regenerative properties within the microenvironment (Mo *et al*, 2002; Mokalled *et al*, 2016; Park *et al*, 2019; Pepe-Mooney *et al*, 2019; Zhao *et al.*, 2008). Such coupling as described here between the Hippo pathway, internalization of receptors, nutrients (including iron) and dynamic forces within the cellular microenvironment likely ensure cell-size distribution homeostasis in a population by modulating growth rates and the duration of cell-division cycles (Cadart, 2019a; Cadart & Heald, 2019; Stewart *et al.*, 2011). This feedback process involves dramatic and rapid changes of the cellular volume and consequently includes changes in intracellular concentrations of solutes and organelles, hence influence directly the rates of chemical reactions occurring in the cell (Cai *et al*, 2010; Delarue *et al*, 2018; Ginzberg *et al*, 2018; Hansen *et al.*, 2015b; Lu *et al*, 2020; Miermont *et al*, 2013; Neurohr *et al*, 2019). Similarly, mechanisms ensure surface-tension homeostasis (Collinet, 2021; Lecuit & Lenne, 2007) couple volume and surface area (Fischer-Friedrich *et al*, 2014; Guo *et al*, 2017). Our data highlight that rapid volume modulation depends on YAP/TAZ and the actin cortex, and suggest that clathrin-dependent endocytosis provides a membrane reservoir, which is coupled to membrane tension. This implies that repeated cycles of rapid internalization, endocytic recycling and exocytosis takes place in order to replenish the plasma membrane. Long-term hydrostatic pressure adaptations are likely caused by YAP/TAZ-mediated transcription of regulators of ion and water fluxes (Fig 2P and EV1 K-M). These examples hint at how dynamic size homeostasis are consequences of intrinsic and extrinsic parameters that drive global growth, and that this needs to be precisely coupled by both biological and physical effects in a healthy individual (Cadart, 2019a, b; Cadart & Heald, 2019). Specialised cell types differ greatly in size, however the size of specific cell types within a given tissue are strikingly similar (Cadart, 2019b; Ginzberg, 2015). Uniformity of the size of particular cell types is a consistent feature of healthy tissues. Consequently, loss of cell size uniformity is a frequent diagnostic marker of malignancy (Dagogo-Jack & Shaw,

2018; Gast *et al*, 2018; Greenough, 1925; Nguyen *et al*, 2016). Cell volume is a fundamental aspect in biology and integrates both the physics and the physiology, including the metabolic state of the cell. Given that YAP/TAZ activation regulate cell growth and proliferation, we speculate that dysregulation of oscillating fluid pressure, likely coupled to the viscoelasticity of the ECM (Chaudhuri *et al*, 2020; Vining & Mooney, 2017; Zanconato *et al.*, 2019), may therefore play a major role in a variety of conditions. For instance, the interplay between YAP/TAZ, oscillating fluid pressure and resistance to cancer treatments could be a confounding factor in solid tumours characterised by an elevated interstitial fluid pressure (Heldin *et al.*, 2004; Moroishi *et al.*, 2015a; Northcott *et al.*, 2018; Stylianopoulos *et al*, 2018); and together with additional factors in the microenvironment drive cancer development and metastasis (Chaudhuri *et al.*, 2020; Fulford *et al.*, 2018; Heldin *et al.*, 2004; Moroishi *et al.*, 2015a; Northcott *et al.*, 2018; Rognoni & Walko, 2019; Salem & Hansen, 2019; Thompson, 2020; Zanconato *et al.*, 2019). The interstitial fluid pressure within the tumour microenvironment drastically increases as a consequence of tumour growth, increased vascular permeability and impaired lymphatic drainage (Northcott *et al.*, 2018). Elevated pressure in solid tumours caused by increased IFP is one of the culprits that impede effective cancer treatment, as it drives cancer proliferation and metastasis, as well as make it challenging to deliver therapeutics to their targets (Ariffin *et al.*, 2014; Heldin *et al.*, 2004; Holle, 2016; Jain *et al*, 2014; Matsubara *et al.*, 2013; Nathan *et al.*, 2005; Nathan *et al.*, 2008). Our findings highlight that the cellular response to fluid pressure via the Hippo pathway is distinct to shear stress, as it is sensed and mediated differently at the plasma membrane. How short-timescale size fluctuations connect to longer term growth and differentiation processes in vivo are still outstanding questions. We hypothesise that such couplings might provide robust feedback loops (Park & Hansen, 2021) into providing steady state cell size control important for organ homeostasis, which are likely important cellular regulators during development (Chan *et al*, 2019), in inflammatory and regenerative processes (Chan & Hiiragi, 2020), and that this dynamic regulation might be chronically altered in tumours (Heldin *et al.*, 2004; Northcott *et al.*, 2018; Wiig & Swartz, 2012). Our work highlights a highly dynamic cellular homeostasis module that is constantly at work in cells. We expect these dynamics are integrated into organ-wide multilevel regulation with potential consequences on physiology and disease. How these dynamics are integrated, between changes in hydrostatic pressure, CDE and the Hippo pathway are not yet fully understood. We speculate cellular sensing of membrane tension and overall cellular volume changes may alter protein condensate levels, and overall spatiotemporal localisation of protein complexes, which together might play coordinating roles in this regulation. It is possible that both subcellular components, integral parts of the plasma membrane, cell-cell and cell-matrix interactions might serve as integrators of this cellular process (Rausch & Hansen, 2020). Our findings offer therapeutically targetable insights into fundamental cellular processes and highlight the intricate dynamics necessary for adaptive cell size regulation within the microenvironment.

Materials and methods

Cell culture

Cell lines were cultured in a humidified incubator at 37°C with 5% CO_2 HEK293A and 143B cells were cultured in DMEM (Gibco) supplemented with 10% heat inactivated FBS (Gibco), 1% (v/v) penicillin-streptomycin (Gibco) and 2mM L-Glutamine (Gibco) unless indicated otherwise. Cells were passaged before cells reached 70-80% confluence using 0.05% Trypsin-EDTA (0.05%) (Gibco). HEK293A wildtype, YAP/TAZ double knockout cells, LATS1/2 double knockout cells, NF2 knockout cells, TEAD1/2/4 triple knockout cells and MST1/2 double knockout cells were obtained from Professor Kun-Liang Guan's lab at the University of California San Diego (UCSD) (Hansen *et al.*, 2015b; Lin *et al.*, 2017; Meng *et al.*, 2015). 143B, osteosarcoma derived cells were obtained from Professor Donald Salter, University of Edinburgh (UoE).

Generation of knockout (KO) cell lines

Guide sequences for *YAP1* and *WWTR1* (encoding TAZ) were annealed to pSpCas9(BB)-2A-Puro (PX459 V2.0; Addgene plasmid #48139) and plasmids were generated using heat-shocked DH5α competent *E. coli* as previously described (Hansen *et al.*, 2015b; Rausch *et al.*, 2019).

Genome edited 143B cells were generated in this study. 143B cells were transfected with plasmids using GenJet *in vitro* transfection reagent (SignaGen Laboratories) and cells were selected with puromycin (Alfa Aesar) 24 hours post transfection for 2-3 days. Puromycin-resistant cells were single-cell sorted into 96-well plates containing growth medium supplemented with 20% total serum concentration at the QMRI Flow Cytometry and Cell Sorting Facility (UoE). Replica plates were generated to allow for screening of KO clones by Western blotting. Confirmed knockout clones were expanded, analysed and frozen down.

Generation of YAP or TAZ re-expression cell lines

Wildtype YAP and S94A mutant YAP stable expression was achieved in HEK293A YAP/TAZ double knockout cells using retroviral transduction. Virus expressing pQCXIH-Myc-YAP or pQCXIH-Myc-YAP S94A plasmids were added to polybrene-treated cells and selected using Hygromycin B (SLS) for YAP re-expressing cell lines. Virus expressing a TAZ WT construct (Rausch *et al.*, 2019; Zhang *et al.*, 2009) were added to polybrene-treated Y/T DKO cells, cells were selected using puromycin to obtain stable cell populations expressing TAZ variants.

Transient transfection of dominant negative AP180 (AP180c)

AP180C is a MYC-tagged carboxy terminal domain of AP180 and acts as a dominant negative mutant of AP180, which inhibits clathrin-dependent endocytosis (Ford *et al.*, 2001). HEK293A cells were seeded at 60-70% confluence in 6-well plates and were transiently transfected with 1 μg of AP180C plasmid using GenJet *in vitro* DNA transfection reagent (SignaGen Laboratories) following the manufacturer's protocol. Experiments investigating the role of clathrin-mediated endocytosis were carried out between 36-40 hours post transfection.

Western blotting

Cells were harvested, and lysates prepared with lysis buffer consisting of pH 6.8 50mM Tris buffer, 2% (w/v) sodium dodecyl sulfate 0.025% (w/v) bromophenol blue,

40% (v/v) glycerol and 5% (v/v) β-mercaptoethanol. Samples were run on SDS-page gels via electrophoresis between 70-110V. PhosTag western blotting, which segregates proteins depending on the degree of phosphorylation, was carried out by supplementing standard 7.5% SDS-PAGE gels with 5mM PhosTag reagent (Wako Chemicals) and 50□M $MnCl_2$. Segregated protein mixtures were then transferred to a PVDF. Enhanced chemiluminescence (Millipore) was used for immunodetection and signal was developed onto X-ray films. Western blots shown are representative of 2-4 biological replicates.

Primary antibodies used to detect proteins of interest were as the following: anti-YAP1 (ab52771) from abcam; anti-YAP1 63.7 (sc101199) this antibody also detects TAZ (Hansen *et al.*, 2015b), anti-CTGF (sc14939), anti-CYR61 (sc13100) and anti-GAPDH sc47724) from Santa Cruz biotechnology, anti-TAZ V387 (4883), anti-pan TEAD (13295S) and anti-pYAP S127 (4911) from Cell Signalling Technology; anti-HSP90 (BD610418) from BD Bioscience. Antibodies were diluted in TBST with 5% BSA at 1:1,000 except anti-GAPDH (1:4,000) and anti-HSP90 (1:10,000).

Secondary antibodies anti-mouse IgG/HRP (P044701), anti-rabbit IgG/HRP (P044801) and anti-goat IgG/HRP (P044901) from Dako were diluted 1:10,000 in 5% milk in TBST.

Quantitative reverse transcription

RNA was extracted from mammalian cells using RNeasy micro kit (Qiagen) following manufacturer's instructions. cDNA synthesis was carried out using High capacity cDNA reverse transcriptase kit (Applied Biosystems). Real-time PCR using 1ng of cDNA/ sample using brilliant III Ultra-Fast SYBR Green qPCR master mix (Agilent technologies) was used to detect relative gene expression levels.

Primer sequences (5' to 3') are as the following:
HPRT1 (fwd AGAATGTCTTGATTGTGGAAGA; rev ACCTTGACCATCTTTGGATTA)
YAP1 (fwd CCAAGGCTTGACCCTCGTTTTG; rev TCGCATCTGTTGCTGCTGGTTG)
WWTR1 (TAZ) (fwd AATGGAGGGCCATATCATTCGAG; rev GTCCTGCGTTTTCTCCTGTATC)
CYR61 (fwd AGCCTCGCATCCTATACAACC; rev TTCTTTCACAAGGCGGCACTC)
CTGF (fwd CCAATGACAACGCCTCCTG; rev TGGTGCAGCCAGAAAGCTC)
CAV1 (fwd GCGACCCTAAACACCTCAAC; rev ATGCCGTCAAAACTGTGTGTC)
LRRC8A (fwd CCTGCCTTGTAAGTGGGTCAC ; rev CACAGCGTCCACGTAGTTGTA)
LRRC8B (fwd CAGCAACTTTTGGCTTCACTAC; rev TGTTTGCCGGAATCTATGTCAG)
LRRC8C (fwd GGGATGTGTTTACCGATTACCTC; rev CTGCACTCTTTTCGGAAGGC)
LRRC8E (fwd CAAGCAGTTCACGGAACAGC; rev GGGCCTCTGATAAGTTCTCCTG)
AQP6 (fwd GTCTTCGCTTCCACCGACAG; rev GCGGGCTGGATTCATGGAG)
AQP11 (fwd GCTCAAAGCGGTCATCACAGA; rev GCCAGCAGGTGGATACGAAG)
TRPV1 (fwd CAGGCTCTATGATCGCAGGAG ; rev TTTGAACTCGTTGTCTGTGAGG)
TRPM7 (fwd ACTGGAGGAGTAAACACAGGT; rev TGGAGCTATTCCGATAGTGCAA)
PIEZO1 (fwd CCGCTCGTTTCCGAGTCAC; rev TGGTAGCAGTAGAGGCAGATG)

Microfluidic setup to alter cellular hydrostatic pressure

A bespoke setup was established consisting of 5% CO_2/air supplied from a gas cylinder (BOC) to OB1 Microfluidic flow controller (Elveflow) to control the air

pressure applied to the input of a μ-Slide I luer 0.4 or μ-Slide VI 0.4 channels (ibidi) containing cells and media, while the output is closed with a stopper. Particular attention was paid to leave no airspace between the stopper and the media. Cells were seeded at 22,000 cells per channel and maintained in 1% FBS complete DMEM throughout the duration of the experiments. Cyclic hydrostatic pressure at 0.1Hz between the range of 100 mbar to 200 mbar was applied to cells.

Transferrin uptake assay

Cells were seeded as described for hydrostatic pump experiments in μ-Slide VI 0.4 channels (ibidi) and maintained at 37°C, 5% CO_2, overnight. Cells were serum-starved for one hour then incubated on ice for 10 minutes in pre-cooled 50 μg/mL transferrin-Alexa 594 (Life technologies). Transferrin uptake was stimulated by incubating cells at steady-state with pre-warmed 50 μg/mL transferrin-Alexa 594 at 37°C or in conjunction with hydrostatic pressure. Surface labelling of transferrin was removed by washing cells with ice-cold stripping buffer (29.2g/L NaCl, 0.5% (v/v) acetic acid in distilled H_2O) twice for 30-40 seconds.

Dextran uptake assay

Cells were seeded as described for hydrostatic pump experiments in μ-Slide VI 0.4 channels (ibidi) and maintained at 37°C, 5% CO_2. overnight. Cells were serum-starved for one hour then incubated on ice with pre-cooled 100 μg/mL dextran Oregon green 488 (Life technologies). Dextran uptake was stimulated using pre-warmed dextran Oregon green 488 and 100ng/mL human recombinant EGF (Gibco) in serum-free DMEM for 10 or 30 minutes at 37°C in conjunction with hydrostatic pressure or at cells at steady-state.

Digital Holographic Microscopy (DHM)

Aforementioned microfluidic set up was coupled to a Digital Holographic Microscope (Phi Lab, Holomonitor M4) to investigate the effect of hydrostatic pressure on cell response in real-time. Time-lapse imaging was acquired for 60s at a rate of 1Hz. Then cells were segmented with the Hstudio Tracking software (Otsu's thresholding) to extract for each cell in the field of view and for each time point quantitative cellular parameters. In particular cell area and mean optical thickness were used to calculate the cellular volume considering a mean cellular index of 1.38 and a mean media refractive index of 1.34. A Matlab script was written to automate calculation of average cell volume at steady state and percentage average change in cell volume in response to hydrostatic pressure.

Flipper-TR and FLIM imaging

Flipper-TR probe was diluted to 2μM in serum-free DMEM and applied to cells 15 minutes prior to imaging. Fluorescent lifetime imaging microscope (FLIM) was used to excite cells at 485 nm and photons were collected through a 600/50 nm bandpass filter. Average fluorescent lifetime measurements were obtained by fitting photon histograms with a double-exponential using the SymPhoTime software, which ensured that chi-squared value was close to 1. The fluorescent lifetime measurements were used as a readout for membrane tension, where lifetime values range between 2.8 – 7.0 ns (Colom *et al.*, 2018). FLIM imaging was conducted at the

Edinburgh Super-Resolution Imaging Consortium (ESRIC) facility branch at Herriot-Watt University.

Drug treatments

Cells were treated with DMSO control or drugs diluted in DMSO at the following concentrations: cells were treated with Latrunculin B (0.5 μM, 2 μM) or Cytochalasin D (0.5 μM, 2 μM; Sigma) for 40 minutes prior to hydrostatic pressure experiments. Nocodazole (3 μ M; abcam) treatment was carried out for 10 minutes. For Cytochalasin D and Nocodazole combination treatment, cells were treated with Cytochalasin D for total length of 40 minutes while Nocodazole for total length of 10 minutes at the aforementioned concentrations. For Torin and Rapamycin treatments, cells were treated at 1 μM and 0.5 μM respectively for total of 40 minutes.

Immunofluorescence imaging (IF)

Cells plated on μ-Slide VI 0.4 channels (ibidi) were in general fixed with prewarmed 37°C 4% paraformaldehyde (PFA) (Thermo Fisher Scientific) in $PBS^{+/+}$ for 20 minutes. For visualisation of tubulin cells were fixed with ice-cold MeOH, as this better preserves the microtule network. PFA (or MeOH) was removed and carefully rinsed with $PBS^{+/+}$. IF blocking buffer (2.5% (v/v) FBS (Life Technologies), 0.3% (v/v) Triton-X-100 in $PBS^{+/+}$) was applied, followed by primary antibody incubation at room temperature (anti-YAP1 (ab52771; abcam; 1:400), Alexa Fluor 488 phalloidin (A12379; Thermo Fisher Scientific; 1:1,000)) for three hours. Cells were incubated with secondary anti-rabbit Immunoglobulin Alexa Fluor 594 (A11037, Thermo Fisher Scientific, 1:400)) for one hour and nuclei was labelled with Hoechst (H3570; Thermo Fisher Scientific, 1:2,000). Labelled cells were imaged using a 63x oil objective on a Leica TCS SP8 MP confocal microscope.

Nuclear-to-cytoplasmic ratio of fluorescence intensity of immunofluorescence images were quantified in Fiji/ImageJ. The nucleus was visualised in the Hoechst channel, and a region of interest (ROI) was determined and used to measure fluorescence intensity in the channel of interest. The same method was carried out to calculate fluorescence intensity in the cytoplasm. For transferrin and dextran measurements, ROI in the cytoplasm was determined by referring to the Hoechst channel and channel of interest. Three ROIs were measured per cell. For all measurements and analysis, cells with multiple nuclei, apoptotic or undergoing mitosis were excluded.

Statistical analysis

Unless otherwise stated, three independent experiments were carried out for each experiment. For statistical tests, Mann-Whitney U test or Kruskal-Wallis test with Dunn's post hoc was conducted. $p=0.05$ was determined as the level of significance for statistical tests.

Data Availability

According to EMBO guidelines, no data that requires deposition in a public database has been generated as part of this study

Author contributions

JP: Conceptualisation; Formal analysis; Investigation; Methodology; Visualization; Writing – original draft; Writing – review & editing. SJ: Investigation. DS: Resources; Supervision. PB: Conceptualisation; Methodology; Resources; Supervision; Funding acquisition; Project administration; Writing – review & editing. CGH: Conceptualisation; Methodology; Resources; Investigation; Supervision; Funding acquisition; Project administration; Writing – original draft; Writing – review & editing. In addition to the CRediT author contributions listed above, the contributions in detail are: JP, PB and CGH designed the study and planned experiments. JP, SJ and CGH performed the experiments. JP and CGH analysed data. DS provided the 143B cells and provided input into the planning of the study. CGH and JP wrote the manuscript with critical input from all the authors.

Disclosure and competing interest statement
The authors declare that they have no conflict of interest.

Acknowledgements
Work ongoing in the Gram Hansen lab is supported by a University of Edinburgh Chancellor's Fellowship and start-up fund, as well as by Worldwide Cancer Research (19-0238) and LifeArc-CSO. This project was initiated by pump prime funding from the Bone Cancer Research Trust (BCRT), Sarcoma UK (SUK202.2016), the Wellcome Trust-University of Edinburgh Institutional Strategic Support Fund (ISSF3) and the Jonathan Haw Fund/ Kinross Trust. J.P. was funded by MRC Precision Medicine DTP Studentship. S.J. by a scholarship from the Chinese Scholarship Council and the Edinburgh Global from University of Edinburgh. We furthermore acknowledge team members for helping with cell culturing and for insightful comments on this study. We acknowledge the technical support and guidance provided by the Centre for Reproductive Health SuRF Histology, Imaging and qPCR Facility staff as well as the QMRI Flow Cytometry and Cell Sorting Facility staff, and Dr Jessica Valli (ESRIC) at Heriot-Watt University for FLIM expertise and imaging. Professor Kun-Liang Guan (UCSD) and Assistant Professor Zhipeng Meng (University of Miami) are acknowledged for sharing gene edited HEK293A cell lines.

References

Akamatsu M, Vasan R, Serwas D, Ferrin MA, Rangamani P, Drubin DG (2020) Principles of self-organization and load adaptation by the actin cytoskeleton during clathrin-mediated endocytosis. *Elife* 9

Ariffin AB, Forde PF, Jahangeer S, Soden DM, Hinchion J (2014) Releasing pressure in tumors: what do we know so far and where do we go from here? A review. *Cancer Res* 74: 2655-2662

Baschieri F, Le Devedec D, Tettarasar S, Elkhatib N, Montagnac G (2020) Frustration of endocytosis potentiates compression-induced receptor signaling. *J Cell Sci* 133

Bertero T, Oldham WM, Cottrill KA, Pisano S, Vanderpool RR, Yu Q, Zhao J, Tai Y, Tang Y, Zhang YY *et al* (2016) Vascular stiffness mechanoactivates YAP/TAZ-

dependent glutaminolysis to drive pulmonary hypertension. *J Clin Invest* 126: 3313-3335
Bitsikas V, Correa IR, Jr., Nichols BJ (2014) Clathrin-independent pathways do not contribute significantly to endocytic flux. *Elife* 3: e03970
Boulant S, Kural C, Zeeh JC, Ubelmann F, Kirchhausen T (2011) Actin dynamics counteract membrane tension during clathrin-mediated endocytosis. *Nat Cell Biol* 13: 1124-1131
Cadart C, Heald R (2019) Cell Biology: The Health Hazards of Super-Sizing. *Curr Biol* 29: R289-R292
Cadart C, Venkova, L., Recho, P., Lagomarsino, M. C., and Piel, M (2019a) The physics of cell-size regulation across timescales. *Nature Physics* 15: 993–1004
Cadart C, Venkova, L., Recho, P., Lagomarsino, M. C., and Piel, M (2019b) The Physics of cell-size regulation across timescales. *Nature Physics* 15: 993-1004
Cai J, Zhang N, Zheng Y, de Wilde RF, Maitra A, Pan D (2010) The Hippo signaling pathway restricts the oncogenic potential of an intestinal regeneration program. *Genes Dev* 24: 2383-2388
Chan CJ, Costanzo M, Ruiz-Herrero T, Monke G, Petrie RJ, Bergert M, Diz-Munoz A, Mahadevan L, Hiiragi T (2019) Hydraulic control of mammalian embryo size and cell fate. *Nature* 571: 112-116
Chan CJ, Hiiragi T (2020) Integration of luminal pressure and signalling in tissue self-organization. *Development* 147
Chaudhuri O, Cooper-White J, Janmey PA, Mooney DJ, Shenoy VB (2020) Effects of extracellular matrix viscoelasticity on cellular behaviour. *Nature* 584: 535-546
Chugh P, Clark AG, Smith MB, Cassani DAD, Dierkes K, Ragab A, Roux PP, Charras G, Salbreux G, Paluch EK (2017) Actin cortex architecture regulates cell surface tension. *Nat Cell Biol* 19: 689-697
Collinet CaL, T. (2021) Programmed and self-organized flow of information during morphogenesis. *Nature Reviews Molecular Cell Biology*
Colom A, Derivery E, Soleimanpour S, Tomba C, Molin MD, Sakai N, Gonzalez-Gaitan M, Matile S, Roux A (2018) A fluorescent membrane tension probe. *Nat Chem* 10: 1118-1125
Coste B, Mathur J, Schmidt M, Earley TJ, Ranade S, Petrus MJ, Dubin AE, Patapoutian A (2010) Piezo1 and Piezo2 are essential components of distinct mechanically activated cation channels. *Science* 330: 55-60
Dagogo-Jack I, Shaw AT (2018) Tumour heterogeneity and resistance to cancer therapies. *Nat Rev Clin Oncol* 15: 81-94
Davis JR, Tapon N (2019) Hippo signalling during development. *Development* 146
Delarue M, Brittingham GP, Pfeffer S, Surovtsev IV, Pinglay S, Kennedy KJ, Schaffer M, Gutierrez JI, Sang D, Poterewicz G *et al* (2018) mTORC1 Controls Phase Separation and the Biophysical Properties of the Cytoplasm by Tuning Crowding. *Cell* 174: 338-349 e320
DuFort CCD (2016) Interstitial Pressure in Pancreatic Ductal Adenocarcinoma Is Dominated by a Gel-Fluid Phase. 110: 2106-2119
Dupont S, Morsut L, Aragona M, Enzo E, Giulitti S, Cordenonsi M, Zanconato F, Le Digabel J, Forcato M, Bicciato S *et al* (2011) Role of YAP/TAZ in mechanotransduction. *Nature* 474: 179-183
Ferguson JP, Huber SD, Willy NM, Aygun E, Goker S, Atabey T, Kural C (2017) Mechanoregulation of clathrin-mediated endocytosis. *J Cell Sci* 130: 3631-3636
Fischer-Friedrich E, Hyman AA, Julicher F, Muller DJ, Helenius J (2014) Quantification of surface tension and internal pressure generated by single mitotic cells. *Sci Rep* 4: 6213
Ford MG, Pearse BM, Higgins MK, Vallis Y, Owen DJ, Gibson A, Hopkins CR, Evans PR, McMahon HT (2001) Simultaneous binding of PtdIns(4,5)P2 and clathrin by AP180 in the nucleation of clathrin lattices on membranes. *Science* 291: 1051-1055

Fulford A, Tapon N, Ribeiro PS (2018) Upstairs, downstairs: spatial regulation of Hippo signalling. *Curr Opin Cell Biol* 51: 22-32
Gast CE, Silk AD, Zarour L, Riegler L, Burkhart JG, Gustafson KT, Parappilly MS, Roh-Johnson M, Goodman JR, Olson B *et al* (2018) Cell fusion potentiates tumor heterogeneity and reveals circulating hybrid cells that correlate with stage and survival. *Sci Adv* 4: eaat7828
Ginzberg MB, Chang N, D'Souza H, Patel N, Kafri R, Kirschner MW (2018) Cell size sensing in animal cells coordinates anabolic growth rates and cell cycle progression to maintain cell size uniformity. *Elife* 7
Ginzberg MH, Kafri, R., and Kirschner, M. (2015) On being the right (cell) size. *Science* 348
Greenough RB (1925) Varying degrees of malignancy in cancer of the breast. *The Journal of Cancer Research* 9: 453–463
Guo M, Pegoraro AF, Mao A, Zhou EH, Arany PR, Han Y, Burnette DT, Jensen MH, Kasza KE, Moore JR *et al* (2017) Cell volume change through water efflux impacts cell stiffness and stem cell fate. *Proc Natl Acad Sci U S A* 114: E8618-E8627
Hansen CG, Moroishi T, Guan KL (2015a) YAP and TAZ: a nexus for Hippo signaling and beyond. *Trends Cell Biol* 25: 499-513
Hansen CG, Ng YL, Lam WL, Plouffe SW, Guan KL (2015b) The Hippo pathway effectors YAP and TAZ promote cell growth by modulating amino acid signaling to mTORC1. *Cell Res* 25: 1299-1313
Hansen CG, Nichols BJ (2009) Molecular mechanisms of clathrin-independent endocytosis. *J Cell Sci* 122: 1713-1721
Hansen CG, Nichols BJ (2010) Exploring the caves: cavins, caveolins and caveolae. *Trends Cell Biol* 20: 177-186
Heldin CH, Rubin K, Pietras K, Ostman A (2004) High interstitial fluid pressure - an obstacle in cancer therapy. *Nature reviews Cancer* 4: 806-813
Holle YaS (2016) In vitro cancer cell–ECM interactions inform in vivo cancer treatment. *Advanced Drug Delivery Reviews* 97: 270-279
Hong AW, Meng Z, Yuan HX, Plouffe SW, Moon S, Kim W, Jho EH, Guan KL (2017) Osmotic stress-induced phosphorylation by NLK at Ser128 activates YAP. *EMBO Rep* 18: 72-86
Huang J, Wu S, Barrera J, Matthews K, Pan D (2005) The Hippo signaling pathway coordinately regulates cell proliferation and apoptosis by inactivating Yorkie, the Drosophila Homolog of YAP. *Cell* 122: 421-434
Huh HD, Kim DH, Jeong HS, Park HW (2019) Regulation of TEAD Transcription Factors in Cancer Biology. *Cells* 8
Jain RK, Martin JD, Stylianopoulos T (2014) The role of mechanical forces in tumor growth and therapy. *Annual review of biomedical engineering* 16: 321-346
Kaksonen M, Roux A (2018) Mechanisms of clathrin-mediated endocytosis. *Nat Rev Mol Cell Biol* 19: 313-326
Kefauver JM, Saotome K, Dubin AE, Pallesen J, Cottrell CA, Cahalan SM, Qiu Z, Hong G, Crowley CS, Whitwam T *et al* (2018) Structure of the human volume regulated anion channel. *Elife* 7
Kim J, Kim YH, Kim J, Park DY, Bae H, Lee DH, Kim KH, Hong SP, Jang SP, Kubota Y *et al* (2017) YAP/TAZ regulates sprouting angiogenesis and vascular barrier maturation. *The Journal of clinical investigation* 127: 3441-3461
Lamar JM, Stern P, Liu H, Schindler JW, Jiang ZG, Hynes RO (2012) The Hippo pathway target, YAP, promotes metastasis through its TEAD-interaction domain. *Proc Natl Acad Sci U S A* 109: E2441-2450
Lecuit T, Lenne PF (2007) Cell surface mechanics and the control of cell shape, tissue patterns and morphogenesis. *Nat Rev Mol Cell Biol* 8: 633-644
Lee HJ, Diaz MF, Price KM, Ozuna JA, Zhang S, Sevick-Muraca EM, Hagan JP, Wenzel PL (2017) Fluid shear stress activates YAP1 to promote cancer cell motility. *Nat Commun* 8: 14122

Li J, Hou B, Tumova S, Muraki K, Bruns A, Ludlow MJ, Sedo A, Hyman AJ, McKeown L, Young RS *et al* (2014a) Piezo1 integration of vascular architecture with physiological force. *Nature* 515: 279-282
Li Q, Li S, Mana-Capelli S, Roth Flach RJ, Danai LV, Amcheslavsky A, Nie Y, Kaneko S, Yao X, Chen X *et al* (2014b) The conserved misshapen-warts-Yorkie pathway acts in enteroblasts to regulate intestinal stem cells in Drosophila. *Dev Cell* 31: 291-304
Li Q, Nirala NK, Nie Y, Chen HJ, Ostroff G, Mao J, Wang Q, Xu L, Ip YT (2018) Ingestion of Food Particles Regulates the Mechanosensing Misshapen-Yorkie Pathway in Drosophila Intestinal Growth. *Dev Cell* 45: 433-449 e436
Li Y, Konstantopoulos K, Zhao R, Mori Y, Sun SX (2020) The importance of water and hydraulic pressure in cell dynamics. *J Cell Sci* 133
Li Z, Zhao B, Wang P, Chen F, Dong Z, Yang H, Guan KL, Xu Y (2010) Structural insights into the YAP and TEAD complex. *Genes & development* 24: 235-240
Liao M, Cao E, Julius D, Cheng Y (2013) Structure of the TRPV1 ion channel determined by electron cryo-microscopy. *Nature* 504: 107-112
Lin KC, Moroishi T, Meng Z, Jeong HS, Plouffe SW, Sekido Y, Han J, Park HW, Guan KL (2017) Regulation of Hippo pathway transcription factor TEAD by p38 MAPK-induced cytoplasmic translocation. *Nature cell biology* 19: 996-1002
Liu CY, Zha ZY, Zhou X, Zhang H, Huang W, Zhao D, Li T, Chan SW, Lim CJ, Hong W *et al* (2010) The hippo tumor pathway promotes TAZ degradation by phosphorylating a phosphodegron and recruiting the SCF{beta}-TrCP E3 ligase. *The Journal of biological chemistry* 285: 37159-37169
Liu F, Lagares D, Choi KM, Stopfer L, Marinkovic A, Vrbanac V, Probst CK, Hiemer SE, Sisson TH, Horowitz JC *et al* (2015) Mechanosignaling through YAP and TAZ drives fibroblast activation and fibrosis. *Am J Physiol Lung Cell Mol Physiol* 308: L344-357
Liu GY, Sabatini DM (2020) mTOR at the nexus of nutrition, growth, ageing and disease. *Nat Rev Mol Cell Biol* 21: 183-203
Lu Y, Wu T, Gutman O, Lu H, Zhou Q, Henis YI, Luo K (2020) Phase separation of TAZ compartmentalizes the transcription machinery to promote gene expression. *Nat Cell Biol* 22: 453-464
Lucas EP, Khanal I, Gaspar P, Fletcher GC, Polesello C, Tapon N, Thompson BJ (2013) The Hippo pathway polarizes the actin cytoskeleton during collective migration of Drosophila border cells. *The Journal of cell biology* 201: 875-885
Malinverno C, Corallino S, Giavazzi F, Bergert M, Li Q, Leoni M, Disanza A, Frittoli E, Oldani A, Martini E *et al* (2017) Endocytic reawakening of motility in jammed epithelia. *Nat Mater* 16: 587-596
Marquet P RB, Magistretti PJ, Cuche E, Emery Y, Colomb T, Depeursinge C. (2005) Digital holographic microscopy: a noninvasive contrast imaging technique allowing quantitative visualization of living cells with subwavelength axial accuracy. *Opt Lett*: 468-470
Mason DE, Collins JM, Dawahare JH, Nguyen TD, Lin Y, Voytik-Harbin SL, Zorlutuna P, Yoder MC, Boerckel JD (2019) YAP and TAZ limit cytoskeletal and focal adhesion maturation to enable persistent cell motility. *The Journal of cell biology* 218: 1369-1389
Matsubara T, Diresta GR, Kakunaga S, Li D, Healey JH (2013) Additive Influence of Extracellular pH, Oxygen Tension, and Pressure on Invasiveness and Survival of Human Osteosarcoma Cells. *Frontiers in oncology* 3: 199
Meng Z, Moroishi T, Mottier-Pavie V, Plouffe SW, Hansen CG, Hong AW, Park HW, Mo JS, Lu W, Lu S *et al* (2015) MAP4K family kinases act in parallel to MST1/2 to activate LATS1/2 in the Hippo pathway. *Nat Commun* 6: 8357
Meng Z, Qiu Y, Lin KC, Kumar A, Placone JK, Fang C, Wang KC, Lu S, Pan M, Hong AW *et al* (2018) RAP2 mediates mechanoresponses of the Hippo pathway. *Nature* 560: 655-660
Miermont A, Waharte F, Hu S, McClean MN, Bottani S, Leon S, Hersen P (2013) Severe osmotic compression triggers a slowdown of intracellular signaling, which

can be explained by molecular crowding. *Proc Natl Acad Sci U S A* 110: 5725-5730
Mirra S, Marfany G, Garcia-Fernandez J (2019) Under pressure: Cerebrospinal fluid contribution to the physiological homeostasis of the eye. *Seminars in cell & developmental biology*
Mo FE, Muntean AG, Chen CC, Stolz DB, Watkins SC, Lau LF (2002) CYR61 (CCN1) is essential for placental development and vascular integrity. *Mol Cell Biol* 22: 8709-8720
Mo JS, Yu FX, Gong R, Brown JH, Guan KL (2012) Regulation of the Hippo-YAP pathway by protease-activated receptors (PARs). *Genes Dev* 26: 2138-2143
Mokalled MH, Patra C, Dickson AL, Endo T, Stainier DY, Poss KD (2016) Injury-induced ctgfa directs glial bridging and spinal cord regeneration in zebrafish. *Science* 354: 630-634
Moreno-Vicente R, Pavon DM, Martin-Padura I, Catala-Montoro M, Diez-Sanchez A, Quilez-Alvarez A, Lopez JA, Sanchez-Alvarez M, Vazquez J, Strippoli R *et al* (2019) Caveolin-1 Modulates Mechanotransduction Responses to Substrate Stiffness through Actin-Dependent Control of YAP. *Cell Rep* 26: 1679-1680
Moroishi T, Hansen CG, Guan KL (2015a) The emerging roles of YAP and TAZ in cancer. *Nat Rev Cancer* 15: 73-79
Moroishi T, Park HW, Qin B, Chen Q, Meng Z, Plouffe SW, Taniguchi K, Yu FX, Karin M, Pan D *et al* (2015b) A YAP/TAZ-induced feedback mechanism regulates Hippo pathway homeostasis. *Genes Dev* 29: 1271-1284
Mugahid D, Kalocsay M, Liu X, Gruver JS, Peshkin L, Kirschner MW (2020) YAP regulates cell size and growth dynamics via non-cell autonomous mediators. *eLife* 9
Myers KA, Rattner JB, Shrive NG, Hart DA (2007) Hydrostatic pressure sensation in cells: integration into the tensegrity model. *Biochem Cell Biol* 85: 543-551
Nakajima H, Yamamoto K, Agarwala S, Terai K, Fukui H, Fukuhara S, Ando K, Miyazaki T, Yokota Y, Schmelzer E *et al* (2017) Flow-Dependent Endothelial YAP Regulation Contributes to Vessel Maintenance. *Dev Cell* 40: 523-536 e526
Nardone G, Oliver-De La Cruz J, Vrbsky J, Martini C, Pribyl J, Skladal P, Pesl M, Caluori G, Pagliari S, Martino F *et al* (2017) YAP regulates cell mechanics by controlling focal adhesion assembly. *Nat Commun* 8: 15321
Nathan SS, DiResta GR, Casas-Ganem JE, Hoang BH, Sowers R, Yang R, Huvos AG, Gorlick R, Healey JH (2005) Elevated physiologic tumor pressure promotes proliferation and chemosensitivity in human osteosarcoma. *Clin Cancer Res* 11: 2389-2397
Nathan SS, Huvos AG, Casas-Ganem JE, Yang R, Linkov I, Sowers R, DiResta GR, Gorlick R, Healey JH (2008) Tumor interstitial fluid pressure may regulate angiogenic factors in osteosarcoma. *Journal of orthopaedic research : official publication of the Orthopaedic Research Society* 26: 1520-1525
Neurohr GE, Terry RL, Lengefeld J, Bonney M, Brittingham GP, Moretto F, Miettinen TP, Vaites LP, Soares LM, Paulo JA *et al* (2019) Excessive Cell Growth Causes Cytoplasm Dilution And Contributes to Senescence. *Cell* 176: 1083-1097 e1018
Nguyen A, Yoshida M, Goodarzi H, Tavazoie SF (2016) Highly variable cancer subpopulations that exhibit enhanced transcriptome variability and metastatic fitness. *Nat Commun* 7: 11246
Northcott JM, Dean IS, Mouw JK, Weaver VM (2018) Feeling Stress: The Mechanics of Cancer Progression and Aggression. *Frontiers in cell and developmental biology* 6: 17
Numata T, Sato-Numata K, Hermosura MC, Mori Y, Okada Y (2021) TRPM7 is an essential regulator for volume-sensitive outwardly rectifying anion channel. *Commun Biol* 4: 599
Ota M, Sasaki H (2008) Mammalian Tead proteins regulate cell proliferation and contact inhibition as transcriptional mediators of Hippo signaling. *Development* 135: 4059-4069

Park HW, Kim YC, Yu B, Moroishi T, Mo JS, Plouffe SW, Meng Z, Lin KC, Yu FX, Alexander CM *et al* (2015) Alternative Wnt Signaling Activates YAP/TAZ. *Cell* 162: 780-794
Park J, Hansen CG (2021) Cellular feedback dynamics and multilevel regulation driven by the hippo pathway. *Biochem Soc Trans* 49: 1515-1527
Park MH, Kim AK, Manandhar S, Oh SY, Jang GH, Kang L, Lee DW, Hyeon DY, Lee SH, Lee HE *et al* (2019) CCN1 interlinks integrin and hippo pathway to autoregulate tip cell activity. *Elife* 8
Pearse BM (1976) Clathrin: a unique protein associated with intracellular transfer of membrane by coated vesicles. *Proc Natl Acad Sci U S A* 73: 1255-1259
Pepe-Mooney BJ, Dill MT, Alemany A, Ordovas-Montanes J, Matsushita Y, Rao A, Sen A, Miyazaki M, Anakk S, Dawson PA *et al* (2019) Single-Cell Analysis of the Liver Epithelium Reveals Dynamic Heterogeneity and an Essential Role for YAP in Homeostasis and Regeneration. *Cell Stem Cell* 25: 23-38 e28
Perez-Gonzalez NA, Rochman ND, Yao K, Tao J, Le MT, Flanary S, Sablich L, Toler B, Crentsil E, Takaesu F *et al* (2019) YAP and TAZ regulate cell volume. *The Journal of cell biology* 218: 3472-3488
Petrilli AM, Fernandez-Valle C (2016) Role of Merlin/NF2 inactivation in tumor biology. *Oncogene* 35: 537-548
Plouffe SW, Lin KC, Moore JL, 3rd, Tan FE, Ma S, Ye Z, Qiu Y, Ren B, Guan KL (2018) The Hippo pathway effector proteins YAP and TAZ have both distinct and overlapping functions in the cell. *The Journal of biological chemistry* 293: 11230-11240
Porazinski S, Wang H, Asaoka Y, Behrndt M, Miyamoto T, Morita H, Hata S, Sasaki T, Krens SFG, Osada Y *et al* (2015) YAP is essential for tissue tension to ensure vertebrate 3D body shape. *Nature* 521: 217-221
Qiao Y, Chen J, Lim YB, Finch-Edmondson ML, Seshachalam VP, Qin L, Jiang T, Low BC, Singh H, Lim CT *et al* (2017) YAP Regulates Actin Dynamics through ARHGAP29 and Promotes Metastasis. *Cell Rep* 19: 1495-1502
Qiu Z, Dubin AE, Mathur J, Tu B, Reddy K, Miraglia LJ, Reinhardt J, Orth AP, Patapoutian A (2014) SWELL1, a plasma membrane protein, is an essential component of volume-regulated anion channel. *Cell* 157: 447-458
Rafiq NBM, Nishimura Y, Plotnikov SV, Thiagarajan V, Zhang Z, Shi S, Natarajan M, Viasnoff V, Kanchanawong P, Jones GE *et al* (2019) A mechano-signalling network linking microtubules, myosin IIA filaments and integrin-based adhesions. *Nat Mater* 18: 638-649
Rausch V, Bostrom JR, Park J, Bravo IR, Feng Y, Hay DC, Link BA, Hansen CG (2019) The Hippo Pathway Regulates Caveolae Expression and Mediates Flow Response via Caveolae. *Curr Biol* 29: 242-255 e246
Rausch V, Hansen CG (2020) The Hippo Pathway, YAP/TAZ, and the Plasma Membrane. *Trends Cell Biol* 30: 32-48
Riggi M, Niewola-Staszkowska K, Chiaruttini N, Colom A, Kusmider B, Mercier V, Soleimanpour S, Stahl M, Matile S, Roux A *et al* (2018) Decrease in plasma membrane tension triggers PtdIns(4,5)P2 phase separation to inactivate TORC2. *Nat Cell Biol* 20: 1043-1051
Rognoni E, Walko G (2019) The Roles of YAP/TAZ and the Hippo Pathway in Healthy and Diseased Skin. *Cells* 8
Saleem M, Morlot S, Hohendahl A, Manzi J, Lenz M, Roux A (2015) A balance between membrane elasticity and polymerization energy sets the shape of spherical clathrin coats. *Nat Commun* 6: 6249
Salem O, Hansen CG (2019) The Hippo Pathway in Prostate Cancer. *Cells* 8
Salmon ED (1975) Pressure-induced depolymerization of brain microtubules in vitro. *Science* 189: 884-886
Sansores-Garcia L, Bossuyt W, Wada K, Yonemura S, Tao C, Sasaki H, Halder G (2011) Modulating F-actin organization induces organ growth by affecting the Hippo pathway. *EMBO J* 30: 2325-2335

Schmitz C, Perraud AL, Johnson CO, Inabe K, Smith MK, Penner R, Kurosaki T, Fleig A, Scharenberg AM (2003) Regulation of vertebrate cellular Mg2+ homeostasis by TRPM7. *Cell* 114: 191-200
Si Y, Ji X, Cao X, Dai X, Xu L, Zhao H, Guo X, Yan H, Zhang H, Zhu C *et al* (2017) Src Inhibits the Hippo Tumor Suppressor Pathway through Tyrosine Phosphorylation of Lats1. *Cancer research* 77: 4868-4880
Steinhardt AA, Gayyed MF, Klein AP, Dong J, Maitra A, Pan D, Montgomery EA, Anders RA (2008) Expression of Yes-associated protein in common solid tumors. *Hum Pathol* 39: 1582-1589
Stewart MP, Helenius J, Toyoda Y, Ramanathan SP, Muller DJ, Hyman AA (2011) Hydrostatic pressure and the actomyosin cortex drive mitotic cell rounding. *Nature* 469: 226-230
Stylianopoulos T, Munn LL, Jain RK (2018) Reengineering the Physical Microenvironment of Tumors to Improve Drug Delivery and Efficacy: From Mathematical Modeling to Bench to Bedside. *Trends Cancer* 4: 292-319
Swartz MA, Lund AW (2012) Lymphatic and interstitial flow in the tumour microenvironment: linking mechanobiology with immunity. *Nat Rev Cancer* 12: 210-219
Taylor MJ, Perrais D, Merrifield CJ (2011) A high precision survey of the molecular dynamics of mammalian clathrin-mediated endocytosis. *PLoS Biol* 9: e1000604
Teng EL, Engler AJ (2019) Mechanical influences on cardiovascular differentiation and disease modeling. *Experimental cell research* 377: 103-108
Thompson BJ (2020) YAP/TAZ: Drivers of Tumor Growth, Metastasis, and Resistance to Therapy. *BioEssays : news and reviews in molecular, cellular and developmental biology*: e1900162
van Helvert S, Storm C, Friedl P (2018) Mechanoreciprocity in cell migration. *Nat Cell Biol* 20: 8-20
Vassilev A, Kaneko KJ, Shu H, Zhao Y, DePamphilis ML (2001) TEAD/TEF transcription factors utilize the activation domain of YAP65, a Src/Yes-associated protein localized in the cytoplasm. *Genes & development* 15: 1229-1241
Vining KH, Mooney DJ (2017) Mechanical forces direct stem cell behaviour in development and regeneration. *Nature reviews Molecular cell biology* 18: 728-742
Voss FK, Ullrich F, Munch J, Lazarow K, Lutter D, Mah N, Andrade-Navarro MA, von Kries JP, Stauber T, Jentsch TJ (2014) Identification of LRRC8 heteromers as an essential component of the volume-regulated anion channel VRAC. *Science* 344: 634-638
Wang L, Luo JY, Li B, Tian XY, Chen LJ, Huang Y, Liu J, Deng D, Lau CW, Wan S *et al* (2016) Integrin-YAP/TAZ-JNK cascade mediates atheroprotective effect of unidirectional shear flow. *Nature* 540: 579-582
Wiig H, Swartz MA (2012) Interstitial fluid and lymph formation and transport: physiological regulation and roles in inflammation and cancer. *Physiol Rev* 92: 1005-1060
Yasui M, Hazama A, Kwon TH, Nielsen S, Guggino WB, Agre P (1999) Rapid gating and anion permeability of an intracellular aquaporin. *Nature* 402: 184-187
Yoshida A, Sakai N, Uekusa Y, Imaoka Y, Itagaki Y, Suzuki Y, Yoshimura SH (2018) Morphological changes of plasma membrane and protein assembly during clathrin-mediated endocytosis. *PLoS Biol* 16: e2004786
Yu FX, Zhao B, Panupinthu N, Jewell JL, Lian I, Wang LH, Zhao J, Yuan H, Tumaneng K, Li H *et al* (2012) Regulation of the Hippo-YAP pathway by G-protein-coupled receptor signaling. *Cell* 150: 780-791
Zanconato F, Cordenonsi M, Piccolo S (2019) YAP and TAZ: a signalling hub of the tumour microenvironment. *Nat Rev Cancer* 19: 454-464
Zhang H, Liu CY, Zha ZY, Zhao B, Yao J, Zhao S, Xiong Y, Lei QY, Guan KL (2009) TEAD transcription factors mediate the function of TAZ in cell growth and epithelial-mesenchymal transition. *J Biol Chem* 284: 13355-13362

Zhang N, Bai H, David KK, Dong J, Zheng Y, Cai J, Giovannini M, Liu P, Anders RA, Pan D (2010) The Merlin/NF2 tumor suppressor functions through the YAP oncoprotein to regulate tissue homeostasis in mammals. *Dev Cell* 19: 27-38
Zhao B, Li L, Tumaneng K, Wang CY, Guan KL (2010) A coordinated phosphorylation by Lats and CK1 regulates YAP stability through SCF(beta-TRCP). *Genes Dev* 24: 72-85
Zhao B, Li L, Wang L, Wang CY, Yu J, Guan KL (2012) Cell detachment activates the Hippo pathway via cytoskeleton reorganization to induce anoikis. *Genes Dev* 26: 54-68
Zhao B, Wei X, Li W, Udan RS, Yang Q, Kim J, Xie J, Ikenoue T, Yu J, Li L *et al* (2007) Inactivation of YAP oncoprotein by the Hippo pathway is involved in cell contact inhibition and tissue growth control. *Genes & development* 21: 2747-2761
Zhao B, Ye X, Yu J, Li L, Li W, Li S, Yu J, Lin JD, Wang CY, Chinnaiyan AM *et al* (2008) TEAD mediates YAP-dependent gene induction and growth control. *Genes Dev* 22: 1962-1971
Zheng Y, Wang W, Liu B, Deng H, Uster E, Pan D (2015) Identification of Happyhour/MAP4K as Alternative Hpo/Mst-like Kinases in the Hippo Kinase Cascade. *Dev Cell* 34: 642-655

Figure Legends

Figure 1. Hydrostatic pressure activates YAP/TAZ.

A PhosTag-based Western blot probed for YAP reveals increased levels of unphosphorylated (downshift) YAP in HEK293A cells in response to cyclic 0.1Hz 200mbar hydrostatic pressure (+) compared to control (-).

B PhosTag-based Western blot probed for TAZ reveals increased levels of unphosphorylated (downshift) TAZ in HEK293A cells in response to cyclic 0.1Hz 200mbar hydrostatic pressure (+) compared to control (-).

C Western blots from cell lysates as in (**A**) and (**B**) show total protein levels in control (-) and in cell lysates obtained from cells exposed to hydrostatic pressure (+) stimulation in HEK293A cells. Note the decrease in the inhibitory p127 YAP signal as well as increase of YAP/TAZ targets CTGF and CYR61 levels upon hydrostatic pressure.

D PhosTag-based Western blot probed for YAP reveals increased levels of unphosphorylated (downshift) YAP in 143B cells in response to hydrostatic pressure (+) compared to control (-).

E Western blot shows total protein levels in control (-) and with hydrostatic pressure (+) stimulation in 143B cells from cell lysates as in D.

F HEK293A cells at steady state (upper) or upon cyclic 0.1Hz 200mbar hydrostatic pressure (lower) were analysed by immunofluorescence. Cells are labelled for Hoechst (blue) and YAP (green). Scale bar = 20μm. Graph on the right depict quantification of nuclear-to-cytoplasmic (Nucl/Cyt) ratio of YAP in cells as shown on the left. Each dot represents a single cell and data are pooled from three independent experiments. Error bars represent mean $\pm$ 95% CI. Mann-Whitney U test. ***$p < 0.001$.

G 143B cells at steady state (upper) or upon cyclic 0.1Hz 200mbar hydrostatic pressure (lower). Graph on the right show quantification of nuclear-to-cytoplasmic (Nucl/Cyt) ratio of YAP in 143B from images as those shown on the left. Each dot

represents a single cell and data are pooled from three independent experiments. Error bars represent mean ± 95% CI. Mann-Whitney U test. ***p < 0.001.
H Western blot confirming no YAP and TAZ expression in two independent (#1 and #2) YAP/TAZ double knockout (Y/T DKO) clones.
I Relative expression levels of YAP/TAZ target genes *CYR61* and *CTGF* in HEK293A WT and Y/T DKO clones in response to cyclic 0.1Hz 200mbar hydrostatic pressure. Data from six independent experiments Error bars represent mean ± SD. Kruskal-Wallis test with Dunn's post hoc. **p=0.0661 (WT *CYR61)*, ***p= 0.0001 (WT *CTGF*), p=0.3924 (Y/T DKO#1 *CYR61*), p=0.4616 (Y/T DKO#1 *CTGF*), p>0.999 (Y/T DKO#2 *CYR61*), p=0.0782 (Y/T DKO#2 *CTGF*).
J *CYR61* and *CTGF* gene expression levels induced by hydrostatic pressure in (**I**) of Y/T DKO #1 and #2 normalised to WT. Kruskal-Wallis test with Dunn's post hoc. *p=0.0259 (Y/T DKO#1 *CYR61*), **p=0.0007 (Y/T DKO#1 *CTGF*), *p=0.0155 (Y/T DKO#2 *CYR61*), ***p<0.001 (Y/T DKO#2 *CTGF*).

Figure 2. YAP/TAZ determine cell size and mediate cellular response to hydrostatic pressure.
A Cell volume of WT and Y/T DKO clones at steady state measured using DHM. Each dot represents a single cell. Error bars represent mean ± 95% CI. Kruskal-Wallis test with Dunn's post-hoc. Data from three independent experiments. ***p<0.001, p=0.0917 (Y/T DKO #1 vs #2).
B Comparison of cell volume of WT and LATS1/2 DKO clones at steady state obtained using DHM. Each dot represents a single cell. Data from three independent experiments. Error bars represent mean ± 95% CI. Kruskal-Wallis test with Dunn's post-hoc. **p=0.0018 (WT vs LATS1/2 DKO #1), ***p<0.001 (WT vs LATS1/2 DKO #2), p=0.0557 (LATS1/2 DKO #1 vs #2).
C Comparison of cell volume of WT and MST1/2 DKO at steady state obtained using DHM. Each dot represents a single cell. Data from three independent experiments. Error bars represent mean ± 95% CI. Mann-Whitney U test. p=0.2731.
D HEK293A NF2 KO cells response to 100mbar cyclic hydrostatic pressure. Each dot represents a single cell and Error bars represent mean ± 95% CI. Data pooled from three independent experiments. Mann-Whitney U test. p=0.4072.
E Comparison of cell volume of WT and TEAD KO clones at steady state obtained using DHM. Each dot represents a single cell. Data from three independent experiments. Error bars represent mean ± 95% CI. Kruskal-Wallis test with Dunn's post-hoc. p>0.9999 for all comparisons.
F Maxima and minima are identified to calculate average percentage change in cell volume in response to hydrostatic pressure using measurements obtained by DHM.
G Representative WT and Y/T DKO single cell volume change in response to hydrostatic pressure recorded by DHM.
H Average change in cell volume in response to hydrostatic pressure in WT and Y/T DKO clones. Each dot represents a single cell. Images and data were acquired at the onset of oscillating pressure. Data from three independent experiments. Error bars represent mean ± 95% CI. Kruskal-Wallis test with Dunn's post hoc. ***p < 0.001 (for both comparisons), p=0.1450 (Y/T DKO #1 vs #2).
I Representative images of Flipper-TR labelled HEK293A WT (top), Y/T DKO #1 (middle) and Y/T DKO #2 (bottom) are shown obtained using fluorescence lifetime imaging microscopy (FLIM) (ex. 485, em. 600)
J Average fluorescence lifetime of Flipper-TR probe quantified using fluorescence lifetime imaging microscope (FLIM) (ex. 485, em. 600). HEK293A wildtype and Y/T DKO clones #1 and #2 were labelled with 2μM Flipper-TR for 15 minutes prior to imaging. The average lifetime measurements were obtained by fitting the photon

histogram with a double exponential and the longest lifetime was extracted to report plasma membrane tension, as previously described (Colom *et al., 2018*). Each dot represents fluorescence lifetime of a single cell and data shown is pooled from three independent experiments (mean±95% CI). Kruskal-Wallis test with Dunn's post hoc. **p=0.0027 (WT vs Y/T DKO#1), *p=0.0136 (WT vs Y/T DKO #2), p>0.9999 (Y/T DKO#1 vs #2).

K Representative immunofluorescence images showing MYC-tagged YAP expression in WT YAP re-expressing cells and S94A mutant YAP re-expressing cells compared to Y/T DKO vector control. 95% were positive for expression of YAP or YAP mutant. Scale bar = 20μm.

L Western blot showing total YAP, TAZ and CYR61 levels in WT YAP and S94A mutant YAP re-expressing cells compared to WT and Y/T DKO vector control.

M Average change in cell volume in response to hydrostatic pressure in WT YAP and S94A mutant YAP re-expressing cells relative to Y/T DKO. Each dot represents a single cell. Error bars represent mean ± 95% CI. Data pooled from three independent experiments. Kruskal-Wallis test with Dunn's post hoc. p<0.001 (vector vs. WT YAP), p=0.4912 (vector vs. S94A YAP), p=0.0327

N Average change in cell volume in response to 100mbar cyclic hydrostatic pressure in WT and TEAD KO clones. Each dot represents a single cell. Data pooled from three independent experiments. Error bars represent mean ± 95% CI. Kruskal-Wallis test with Dunn's post hoc. ***p < 0.001 (for both comparisons), p>0.9999 (TEAD KO #1 vs #2).

O WT and Y/T DKO cell volume were measured at steady-state and the average change in cell volume was quantified using the DHM as in previous experiments, these are labelled (-). Cells were then subjected to cyclic hydrostatic pressure for 2 hours and their cell volume was quantified to determine whether prior exposure to hydrostatic pressure ('pre-conditioning') would change their cell volume response, these are labelled (+). Each dot represents a single cell and error bars represent 95% CI. Graphs include data obtained from four independent experiments. Kruskal-Wallis with Dunn's post hoc. ns= p>0.9999.

P The average percentage change in cell volume was quantified under the same experimental conditions as in "O". The average change in cell volume in response to cyclic hydrostatic pressure of cells with no previous exposure to hydrostatic pressure (labelled as (-)) was quantified using DHM and compared to those with prior exposure to hydrostatic pressure (labelled (+)). Each dot represents a single cell and error bars represent 95% CI. Graphs include data obtained from four independent experiments. Kruskal-Wallis with Dunn's post hoc. **p=0.006 (WT), p=0.4173 (Y/T DKO), ns= p>0.9999.

Figure 3. Cellular response to hydrostatic pressure is regulated by the actin cytoskeleton.

A Cell volume measured by DHM of HEK293A cells treated with 0.5μM (left) and 2μM (right) Cytochalasin D. Each dot represents a single cell and error bars represent mean ± 95% CI. Data pooled from four independent experiments. Mann-Whitney U test. **p=0.0033 (WT 0.5 μM), ***p<0.001 (Y/T DKO 0.5 μM), ***p=0.004(LATS1/2 DKO 0.5μM), ***p<0.001 (WT 2μM), **p=0.0022 (Y/T DKO 2μM), *p=0.0145 (LATS1/2 DKO 2μM).

B Fold change in cell volume upon treatment with 0.5μM (left) and 2μM (right) Cytochalasin D relative to untreated control. Each dot represents a single cell and error bars represent mean ± 95% CI. Data pooled from four independent experiments. Mann-Whitney U test. p=0.1197 (WT vs Y/T DKO), p>0.9999 (all other comparisons).
C Representative immunofluorescence images showing Phalloidin-labelled actin (red) and Hoechst (blue) in Latrunculin B (LatB) (0.5μM) or Cytochalasin D (CytD) (2μM)-treated HEK293A cells compared to control across Hippo pathway genome-edited cells as shown. Scale bar = 20μm.
D Average change in cell volume obtained by DHM in response to hydrostatic pressure with 2μM Cytochalasin D (CytD) treatment in WT, Y/T DKO and LATS1/2 DKO cells. Each dot represents a single cell and error bars represent mean ± 95% CI. Data pooled from four independent experiments. Kruskal-Wallis test with Dunn's post hoc. **p=0.0044 (WT con vs CytD), p*=0.0409 (Y/T DKO con vs CytD), p>0.9999 (LATS1/2 DKO con vs CytD), ***p=0.0003 (WT con vs Y/T DKO con), ***p<0.001 (WT con vs Y/T DKO CytD), ***p<0.001 (Y/T DKO CytD vs LATS1/2 DKO CytD).
E Fold difference in average change in cell volume in response to dynamic hydrostatic pressure from (**H**) normalised against untreated cells. Each dot represents a single cell and error bars are 95% CI. Mann-Whitney U test. **p=0.0069 (WT vs. Y/T DKO), **p=0.0031 (WT vs LATS1/2 DKO).
F Average change in cell volume in response to hydrostatic pressure with 0.5μM Latrunculin B (Lat B) treatment in WT, Y/T DKO and LATS1/2 DKO cells. Each dot represents a single cell and error bars represent mean ± 95% CI. Data pooled from four independent experiments. Kruskal-Wallis test with Dunn's post hoc. ***p<0.001 (all comparisons), p=0.0972 (LATS/12 DKO con vs LatB), *p=0.0216 (Y/T DKO LatB vs LATS1/2 DKO LatB).
G Fold difference in average change in cell volume in response to cyclic 0.1Hz 100mbar hydrostatic pressure from (**F**) normalised against control. Each dot represents a single cell and error bars represent mean ± 95% CI. Mann-Whitney U test. p=0.1472 (WT vs. Y/T DKO), **p=0.0015 (WT vs LATS1/2 DKO).

Figure 4. Disruption of microtubules has no effect on cellular response to hydrostatic pressure in WT and Y/T DKO cells.
A Confocal IF images labelled with Hoechst (Blue) and Alpha-tubulin (green) showing loss of microtubule structures in response to 10 min nocodazole (NCD) treatment in WT, Y/T DKO and LATS1/2 DKO cells. Scale bar = 20μm.
B Confocal IF images labelled with Hoechst (blue) and phalloidin (red) visualising the actin cytoskeleton organisation in response to NCD treatment. Scale bar = 10μm.
C Steady-state cell volume of Nocodazole-treated cells compared to control. Each dot represents a single cell and data pooled from five independent experiments. Error bars represent mean ± 95% CI. Mann-Whitney U test. p=0.1925 (WT), p=0.9008 (Y/T DKO), p=0.1375 (LATS1/2 DKO).
D Cell response to hydrostatic pressure after 10 min NCD treatment compared to control. Each dot represents a single cell and data pooled from five independent experiments. Error bars represent mean ± 95% CI. Mann-Whitney U test. p=0.4240 (WT), p=0.7567 (Y/T DKO), ***p<0.001 (LATS1/2 DKO).

E Cell response to hydrostatic pressure after CytD (40 min) and NCD (10 min) treatment compared to control. Each dot represents a single cell and data pooled from four independent experiments. Error bars represent mean ± 95% CI. Mann-Whitney U test. ***p<0.001 (WT), p>0.9999 (LATS1/2 DKO).

Figure 5. Hydrostatic pressure promotes clathrin-dependent internalisation.
A Confocal IF images labelled with Hoechst (Blue) and internalised Transferrin (Trf). Cells were allowed to internalize for ten minutes, fixed and acid stripped to remove surface bound Trf. Hydrostatic pressure (H.P.) promotes transferrin uptake in WT and LATS1/2 DKO cells. Scale bar = 20μm.
B Quantification of transferrin uptake in WT, Y/T DKO and LATS1/2 DKO cells treated with hydrostatic pressure compared to steady state. Each dot represents a single cell and error bars represent mean ± 95% CI. Data from four independent experiments. Kruskal-Wallis test with Dunn's post hoc. Steady-state statistical analysis is shown in blue, transferrin uptake induced by pressure is shown in black. ***p<0.001 (WT con vs +H.P.), p=0.2375 (Y/T DKO con vs +H.P.), ***p<0.001 (LATS1/2 DKO con vs +H.P.), p=0.2764 (WT con vs Y/T DKO con), p=0.0808 (WT con vs LATS1/2 DKO con), ***p=0.0004 (Y/T DKO con vs LATS1/2 DKO con).
C Confocal IF images myc tagged AP180C (green) cells showing internalised Trf (red) and stained with Hoechst (blue). AP180C inhibits transferrin uptake in WT and Y/T DKO cells. Scale bar = 20μm.
D Quantification of transferrin uptake in AP180C positive cells compared to vector control from images as in C. Each dot represents a single cell from four independent experiments and error bars represent mean ± 95% CI. Mann-Whitney U test. ***p < 0.001 (for both comparisons).
E Confocal IF images of HEK293A WT cells showing subcellular localisation of YAP (red) in AP180C (green) negative and positive WT and LATS1/2 DKO cells. Cells also stained with Hoechst (blue).
F Quantification of cytoplasmic-to-nuclear ratio of YAP in AP180C positive WT and LATS1/2 DKO cells compared to vector control from images as in **E**. Each dot represents a single cell pooled from four independent experiments. Error bars represent mean ± 95% CI. Mann-Whitney U test. ***p=0.0008 (WT), p=0.9318 (LATS1/2 DKO).
G Cell response to hydrostatic pressure with AP180C-mediated inhibition of clathrin-dependent endocytosis. Each dot represents a single cell pooled from four independent experiments. Error bars represent mean ± 95% CI. Data pooled from four independent experiments. Kruskal-Wallis test with Dunn's post hoc. ***p=0.0005 (WT), p=0.3930 (Y/T DKO), p=0.2929 (LATS1/2 DKO).

Figure 6. Summary of cellular response to hydrostatic pressure.

Expanded View (EV) Figure legends

Figure EV1.
A PhosTag-based Western blot probed for YAP reveals no changes in YAP phosphorylation levels in HEK293A and 143B cells in response to static 500mbar hydrostatic pressure (+) compared to control (-).

B Western blot showing LATS1 and LATS2 levels in WT and LATS1/2 DKO cells.
C Western blot showing NF2 expression level in WT and NF2 KO cells.
D Western blot showing TEAD expression level in WT and TEAD KO cells.
E Western blot showing YAP, TAZ and CYR61 levels in 143B YAP KO and TAZ KO cells relative to WT.
F 143B WT, YAP KO and TAZ KO response to 100mbar cyclic hydrostatic pressure as measured by DHM. Each dot represents a single cell from three independent experiments and error bars represent mean ± 95% CI. Mann-Whitney U test. ***p<0.001 (WT vs YAP KO), ***p=0.006 (WT vs TAZ KO).
G Steady state volume of Y/T DKO relative to WT YAP and S94A mutant YAP re-expressing Y/T DKO cells as measured by DHM. Each dot represents a single cell from three independent experiments and error bars represent 95% CI. Kruskal-Wallis test with Dunn's post hoc. p>0.999 (vector vs WT YAP), p=0.2173 (vector vs S94A YAP), p=0.9837 (WT YAP vs S94A YAP).
H Western blot showing total YAP, TAZ and CYR61 levels in WT TAZ re-expressing cells compared to WT and Y/T DKO vector control.
I Steady-state cell volume WT TAZ re-expressing cells relative to Y/T DKO as imaged and analysed by DHM. Each dot represents a single cell from three independent experiments. Error bars represent mean ± 95% CI. Mann-Whitney U test. ***p < 0.001.
J Average change in cell volume in response to hydrostatic pressure in WT TAZ re-expressing cells relative to Y/T DKO as imaged and analysed by DHM. Each dot represents a single cell from three independent experiments. Error bars represent mean ± 95% CI. Mann-Whitney U test. ***p < 0.001.
K Candidate genes conferring YAP/TAZ-mediated cellular response to hydrostatic pressure. Gene expression levels of HEK293A WT cells in response to 0.1Hz, 200mbar cyclic hydrostatic pressure (4 hours) compared with steady-state levels within each genotype and analysed by RT-qPCR. Graphs show data obtained from four independent experiments. Error bars represent mean ± SD. Kruskal-Wallis test with Dunn's post hoc.
L Gene expression level induced by hydrostatic pressure in Y/T DKO#1 cells normalised to WT levels. Graphs show data obtained from four independent experiments. Error bars represent mean ± SD. Kruskal-Wallis test with Dunn's post hoc.
M Gene expression level induced by hydrostatic pressure in Y/T DKO#2 cells normalised to WT levels. Graphs show data obtained from four independent experiments. Error bars represent mean ± SD. Kruskal-Wallis test with Dunn's post hoc.

Figure EV2.
A Average change in cell volume in response to 100mbar cyclic hydrostatic pressure in WT and LATS1/2 DKO clones. Each dot represents a single cell. Data pooled from three independent experiments. Error bars represent mean ± 95% CI. Kruskal-Wallis test with Dunn's post hoc. p>0.9999 (for all comparisons).
B Average change in cell volume in response to 100mbar cyclic hydrostatic pressure in WT and MST1/2 DKO. Each dot represents a single cell. Data pooled from three

independent experiments Error bars represent mean ± 95% CI. Mann-Whitney U test. p=0.0781.

C HEK293A NF2 KO steady-state volume compared to WT cells. Each dot represents a single cell and Error bars represent mean ± 95% CI. Data pooled from three independent experiments. Mann-Whitney U test. ***p < 0.001.

D PhosTag based western blot probing for YAP reveals dephosphorylation of YAP in response to 0.5μM Latrunculin B (LB) and 2μM Cytochalasin D (CD) treatment in WT cells.

E Comparison of average change in cell volume measured by DHM in response to 100mbar cyclic hydrostatic pressure with 2μM Latrunculin B treatment in WT, Y/T DKO and LATS1/2 DKO cells. Each cell represents a single cell and error bars represent mean ± 95% CI. Data pooled from four independent experiments. Mann-Whitney U test. ***p<0.001 (WT), ***p<0.001 (Y/T DKO), *p=0.0331 (LATS1/2 DKO).

F Comparison of average change in cell volume in response to 100mbar cyclic hydrostatic pressure with 0.5μM Cytochalasin D treatment in WT, Y/T DKO and LATS1/2 DKO cells. Each cell represents a single cell and error bars represent mean ± 95% CI. Data pooled from four independent experiments. Mann-Whitney U test. p=0.2021 (WT), **p=0.0035 (Y/T DKO), p=0.9148 (LATS1/2 DKO).

G Fold difference in average change in cell volume in response to hydrostatic pressure from B normalised against cells not treated with 2μM Latrunculin B. Each dot represents a single cell and error bars are 95% CI. Mann-Whitney U test. p>0.9999 (WT vs Y/T DKO), p=0.0723 (WT vs LATS1/2 DKO).

H Fold difference in average change in cell volume in response to hydrostatic pressure from C normalised against cells not treated with 0.5μM Cytochalasin D. Each dot represents a single cell and error bars represent mean ± 95% CI. Mann-Whitney U test. p=0.4619 (WT vs Y/T DKO), p=0.7087 (WT vs LATS1/2 DKO).

I HEK293A YAP/TAZ DKO and LATS1/2 DKO clone #2's responses to cyclic 0.1Hz 200mbar dynamic hydrostatic pressure with AP180C-mediated inhibition of clathrin-dependent endocytosis. Each dot represents a single cell and error bars represent mean ± 95% CI. Data pooled from four independent experiments. Kruskal-Wallis test with Dunn's post hoc. ***p < 0.001 (WT), p=0.2522 (Y/T DKO), p=0.0612 (LATS1/2 DKO).

Figure EV3.

A Lysates from cells treated for 40 minutes with Torin (1μM) or Rapamycin (0.5μM) compared to control cells were analysed by immunoblots for the levels of the mTORC1 substrate S6K, pS6K and GAPDH (loading control). Note the levels of pS6K is drastically decreased in Torin and Rapamycin treated HEK293A cells, highlighting that these drugs effectively inhibits S6K phosphorylation.

B Cells treated with Torin (1μM) and Rapamycin (0.5μM) as in A) and analysed by DHM to obtain their optical cellular volume. Each dot represents a single cell from three independent experiments. 40 minutes Torin or Rapamycin treatment does not affect steady-state cell volume. Error bars represent mean ± 95% CI. Kruskal-Wallis test with Dunn's post-hoc. p=0.5709 (con vs Torin), p>0.9999 (con vs Rapamycin), p>0.9999 (Torin vs Rapamycin).

C WT cells treated with Torin (1μM) and Rapamycin (0.5μM) as in A) and imaged using DHM while being subjected to cyclic 0.1Hz 100mbar fluid pressure. 40 minutes

Torin (1μM) and Rapamycin (0.5μM) treatment has no effect on cell volume changes in response to hydrostatic pressure. Each dot represents a single cell from three independent experiments. Error bars represent mean ± 95% CI. Kruskal-Wallis test with Dunn's post-hoc. p=0.5321 (con vs Torin), p>0.9999 (con vs Rapamycin), p=0.4860 (Torin vs Rapamycin).
D Western blot confirming no CAV1 protein expression in CAV1 KO HEK293A cells.
E CAV1 KO cellular response to cyclic 0.1Hz 200mbar hydrostatic pressure compared to WT. Each dot represents a single cell from three independent experiments and error bars represent mean ± 95% CI. Mann-Whitney U test. p=0.4904.
F Relative *CAV1* expression levels of CAV1 knockdown clone #1 and #2 from four independent experiments. Mann-Whitney U test. Error bars represent mean ± SD. **p=0.0079.
G Western blot confirming reduction of total CAV1 protein levels in shCAV1 clones #1 and #2.
H shRNA CAV1 knockdown cell response to cyclic 0.1Hz 100mbar hydrostatic pressure compared to WT. Each dot represents a single cell and error bars represent mean ± 95% CI. Data pooled from four independent experiments. Kruskal-Wallis test with Dunn's post hoc. p>0.9999 (vector vs shCAV#1), p=0.1892 (vector shCAV#2), p=0.0812 (shCAV#1 vs shCAV#2).

Figure EV4.
A Confocal image of fluorescently labelled transferrin (red) uptake by 143B cells under steady-state conditions and in response to cyclic 0.1Hz 200mbar hydrostatic pressure. Cells labelled for Hoechst (blue). Scale bar = 20μm.
B Quantification of transferrin uptake in 143B cells treated with hydrostatic pressure compared to steady state from images as in A. Each dot represents a single cell and error bars represent mean ± 95% CI. Data from four independent experiments. Mann-Whitney U test. *** p< 0.001.
C Confocal IF images of HEK293A cells. Cells are labelled with Dextran (green) and Hoechst (blue). HEK293A WT dextran uptake in response to 10 min (left) and 30 min (right) cyclic hydrostatic pressure compared to steady state (Con). Scale bar = 20μm.
D Confocal images of Y/T DKO HEK293A cells. Cells are labelled with Dextran (green) and Hoechst (blue). Y/T DKO HEK293A dextran uptake in response to 10 min (left) and 30 min (right) cyclic hydrostatic pressure compared to steady state (Con). Scale bar = 20μm.
E Confocal images of LATS1/2 DKO HEK293A cells. Cells are labelled with Dextran (green) and Hoechst (blue). LATS1/2 DKO HEK293A dextran uptake in response to 10 min (left) and 30 min (right) cyclic hydrostatic pressure compared to steady state (Con). Scale bar = 20μm.
F Changes in Dextran signal (30 min uptake) in response to cyclic hydrostatic pressure compared to control in WT, Y/T DKO and LATS1/2 DKO. Data obtained from images as in A-C. Each dot represents a single cell from three independent experiments. Error bars represent mean ± 95% CI. Data points obtained from images as in A-C. Kruskal-Wallis test with Dunn's post hoc. p=0.1406 (WT), p=0.6850 (Y/T DKO), p>0.9999 (LATS1/2 DKO).

G Dextran uptake (30 min) at steady-state in Y/T DKO and LATS1/2 DKO cells relative to WT steady-state. Each dot represents a single cell from three independent experiments. Data points obtained from images as in A-C. Error bars represent mean ± 95% CI. Mann-Whitney U test. p>0.9999.
H Dextran uptake (30 min) in response to hydrostatic pressure relative to steady state. Each dot represents a single cell from three independent experiments. Error bars represent mean ± 95% CI. Kruskal-Wallis test with Dunn's post hoc. p=0.0542 (WT vs Y/T DKO), p=0.8633 (WT vs LATS1/2 DKO), p=0.5795 (Y/T DKO vs LATS1/2 DKO).

Figure EV5.
A-F PhosTag probing from HA-tagged YAP levels in AP180C transfection positive cells. Vector or AP180C plasmid was co-transfected with HA-YAP and YAP activation status in response to hydrostatic pressure is shown (PhosTag gel). Anti-HA tag antibody was used to probe for HA-tagged YAP. YAP phosphorylation levels in HEK293A **A** WT, **B** LATS1/2 DKO, **C** MST1/2 DKO, **D** M4K4/6/7 KO (M4K KO), **E** MST1/2-M4K4/6/7 KO (5KO) and **F** MST1/2-M4K1/2/3/4/6/7 KO (8KO) cells are shown.
G Immunofluorescence images show AP180C positive cells in green and YAP in red. Hoechst highlights the nucleus (shown in blue). AP180C promotes nuclear exclusion of YAP in M4K KO but not MST1/2 DKO cells. Cells were transfected with Myc-tagged AP180C and the subcellular localisation of YAP was examined in response to hydrostatic pressure. Scale bar = 20μm.
H Quantification of nuclear to cytoplasmic ratio (Nucl/Cyt) of YAP in AP180C transfection positive cells compared to control using images as shown in **G**. Each dot represents a single cell and error bars are mean ± 95% CI. Graph shows data obtained from three independent experiments. Mann-Whitney U test. p=0.3516 (MST1/2 DKO), p=0.0001 (M4K KO).

Figure 1

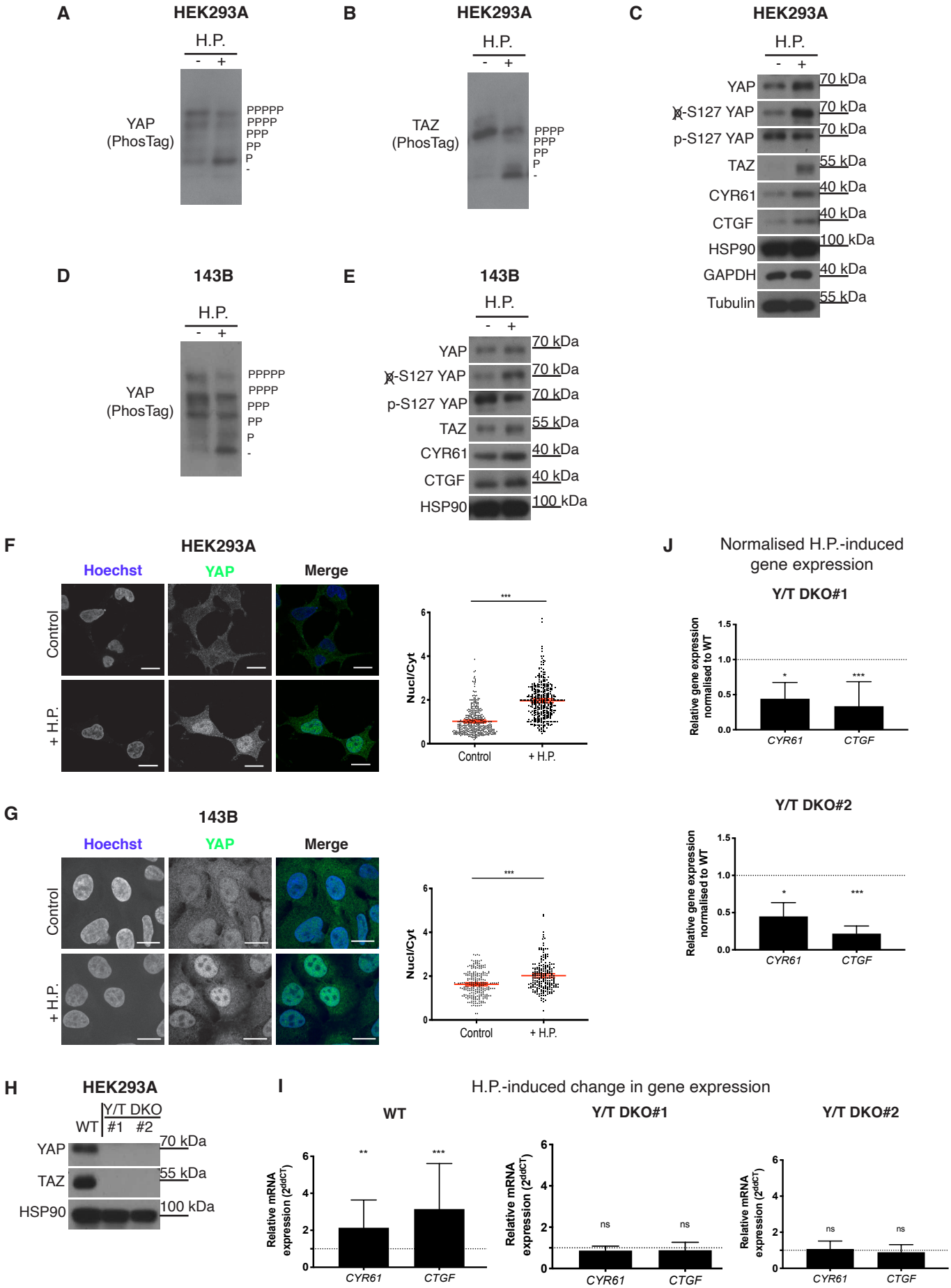
A
HEK293A
H.P.
- +
YAP
(PhosTag)
PPPPP
PPPP
PPP
PP
P
-
B
HEK293A
H.P.
- +
TAZ
(PhosTag)
PPPP
PPP
PP
P
-
C
HEK293A
H.P.
- +
YAP
p-S127 YAP
p-S127 YAP
TAZ
CYR61
CTGF
HSP90
GAPDH
Tubulin
70 kDa
70 kDa
70 kDa
55 kDa
40 kDa
40 kDa
100 kDa
40 kDa
55 kDa
D
143B
H.P.
- +
YAP
(PhosTag)
PPPPP
PPPP
PPP
PP
P
-
E
143B
H.P.
- +
YAP
p-S127 YAP
p-S127 YAP
TAZ
CYR61
CTGF
HSP90
70 kDa
70 kDa
70 kDa
55 kDa
40 kDa
40 kDa
100 kDa
F
HEK293A
Hoechst
YAP
Merge
Control
+ H.P.
Nucl/Cyt
***
Control
+ H.P.
G
143B
Hoechst
YAP
Merge
Control
+ H.P.
Nucl/Cyt
***
Control
+ H.P.
J
Normalised H.P.-induced gene expression
Y/T DKO#1
Relative gene expression normalised to WT
CYR61
CTGF
Y/T DKO#2
Relative gene expression normalised to WT
CYR61
CTGF
H
HEK293A
WT
Y/T DKO #1 #2
YAP
TAZ
HSP90
70 kDa
55 kDa
100 kDa
I
H.P.-induced change in gene expression
WT
Y/T DKO#1
Y/T DKO#2
Relative mRNA expression (2ddCT)
CYR61
CTGF
ns

Figure 2

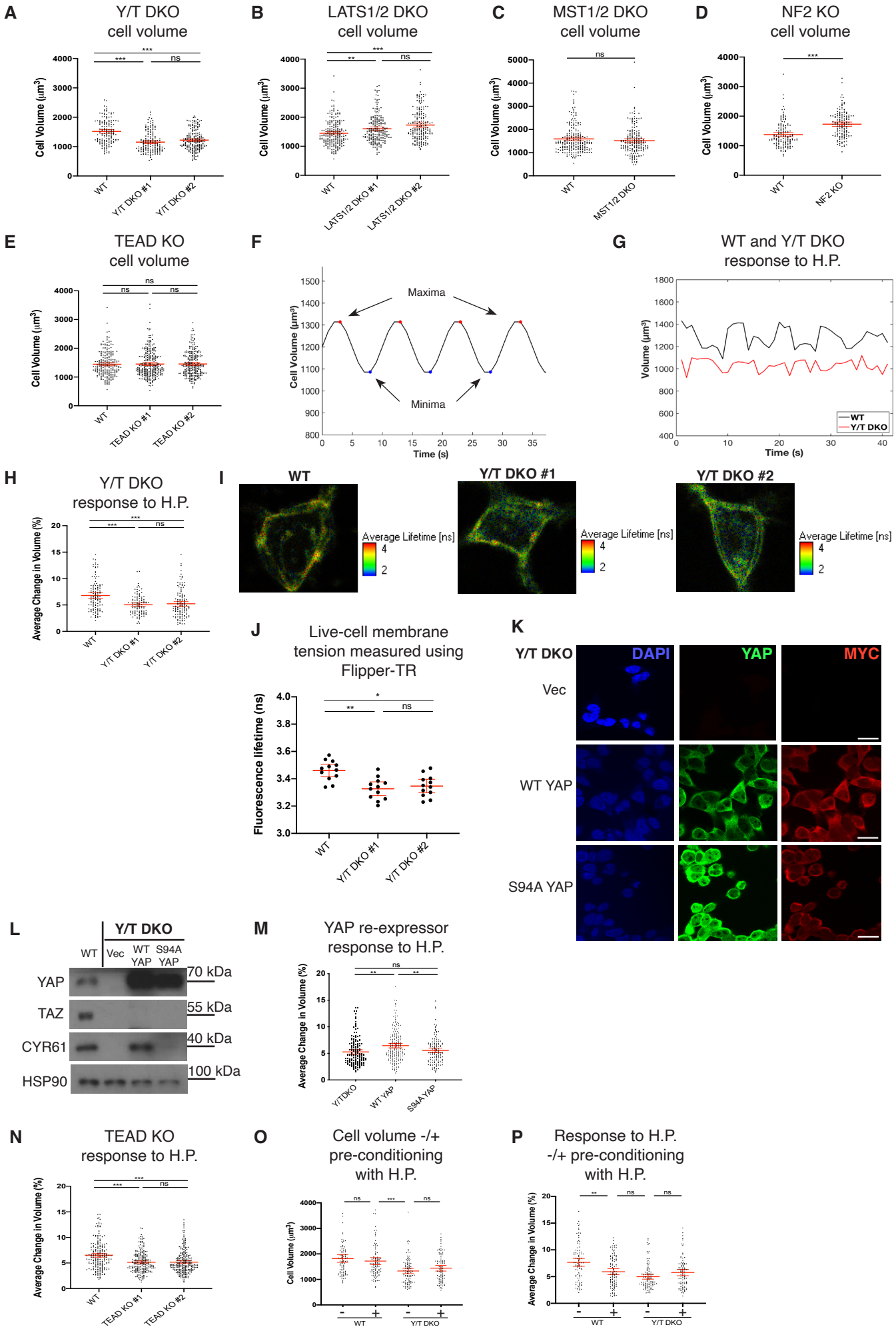
A
Y/T DKO
cell volume
Cell Volume (μm³)
WT
Y/T DKO #1
Y/T DKO #2
B
LATS1/2 DKO
cell volume
LATS1/2 DKO #1
LATS1/2 DKO #2
C
MST1/2 DKO
cell volume
MST1/2 DKO
D
NF2 KO
cell volume
NF2 KO
E
TEAD KO
cell volume
TEAD KO #1
TEAD KO #2
F
Maxima
Minima
Time (s)
G
WT and Y/T DKO
response to H.P.
Volume (μm³)
WT
Y/T DKO
H
Y/T DKO
response to H.P.
Average Change in Volume (%)
I
WT
Y/T DKO #1
Y/T DKO #2
Average Lifetime [ns]
J
Live-cell membrane
tension measured using
Flipper-TR
Fluorescence lifetime (ns)
K
Y/T DKO
DAPI
YAP
MYC
Vec
WT YAP
S94A YAP
L
Y/T DKO
WT
Vec
WT YAP
S94A YAP
YAP
TAZ
CYR61
HSP90
70 kDa
55 kDa
40 kDa
100 kDa
M
YAP re-expressor
response to H.P.
Y/TDKO
WT YAP
S94A YAP
N
TEAD KO
response to H.P.
O
Cell volume -/+
pre-conditioning
with H.P.
P
Response to H.P.
-/+ pre-conditioning
with H.P.

Figure 3

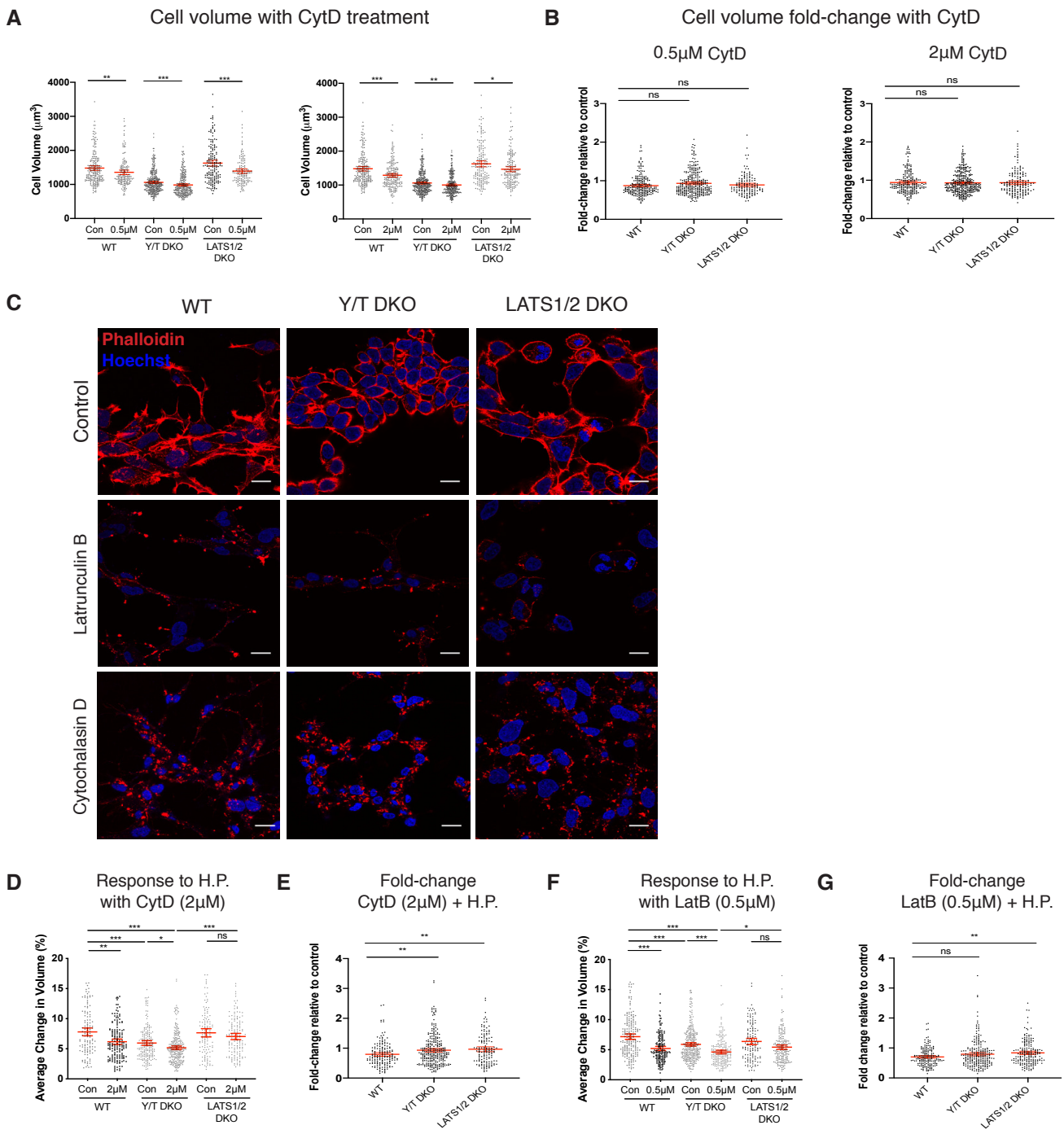
A
Cell volume with CytD treatment
Cell Volume (μm³)
Con 0.5μM Con 0.5μM Con 0.5μM
WT Y/T DKO LATS1/2 DKO
Con 2μM Con 2μM Con 2μM
WT Y/T DKO LATS1/2 DKO
B
Cell volume fold-change with CytD
0.5μM CytD
2μM CytD
Fold-change relative to control
WT Y/T DKO LATS1/2 DKO
C
WT
Y/T DKO
LATS1/2 DKO
Phalloidin
Hoechst
Control
Latrunculin B
Cytochalasin D
D
Response to H.P. with CytD (2μM)
Average Change in Volume (%)
E
Fold-change CytD (2μM) + H.P.
F
Response to H.P. with LatB (0.5μM)
G
Fold-change LatB (0.5μM) + H.P.
Fold change relative to control

Figure 4

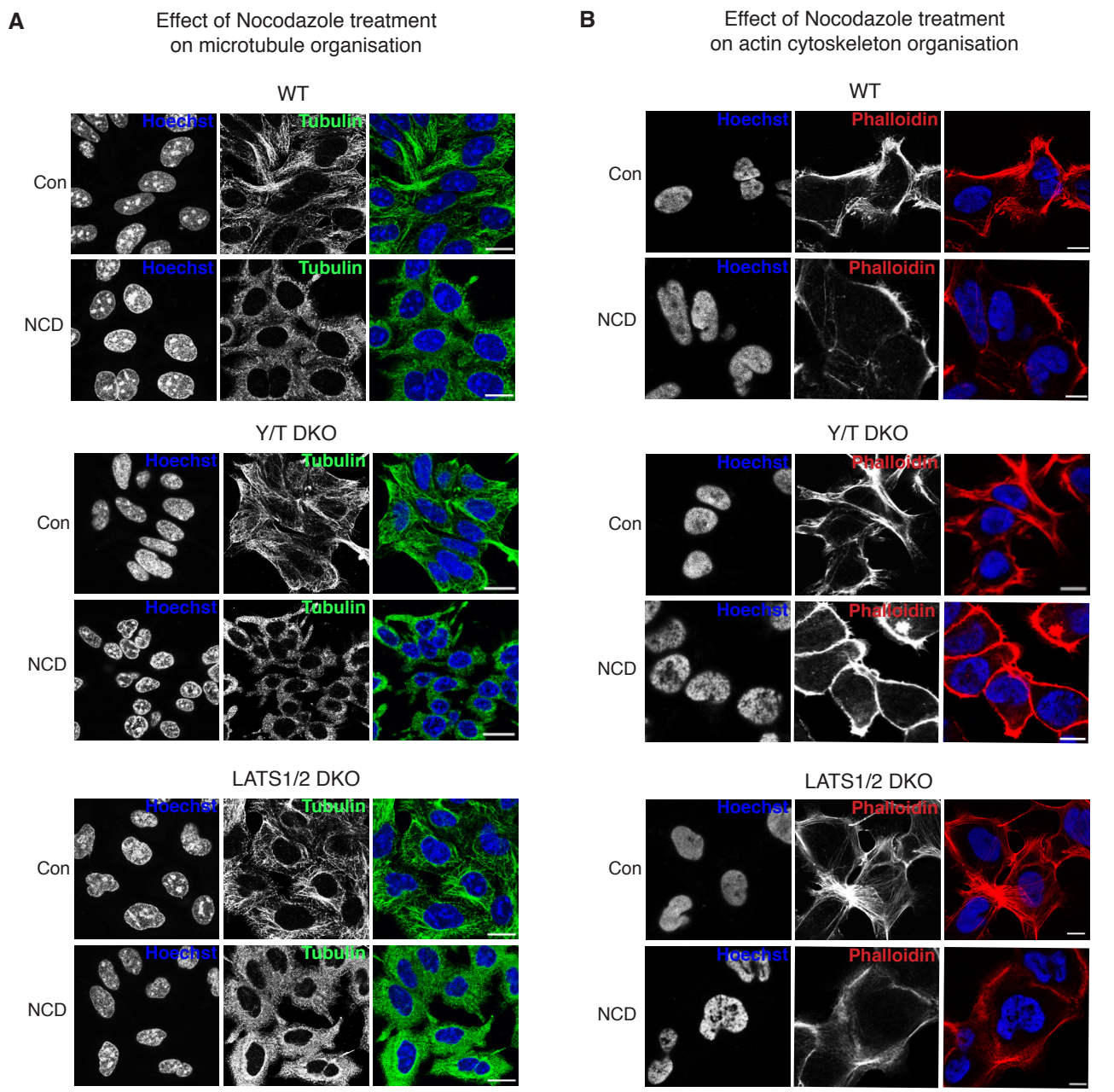
A
Effect of Nocodazole treatment
on microtubule organisation
WT
Con
NCD
Hoechst
Tubulin
Y/T DKO
LATS1/2 DKO
B
Effect of Nocodazole treatment
on actin cytoskeleton organisation
Phalloidin

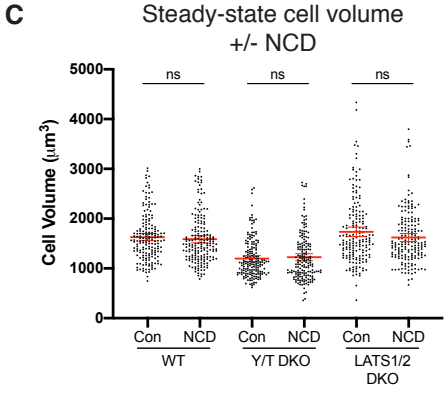
C
Steady-state cell volume
+/- NCD
Cell Volume (μm³)
5000
4000
3000
2000
1000
0
ns
Con
NCD
WT
Y/T DKO
LATS1/2
DKO

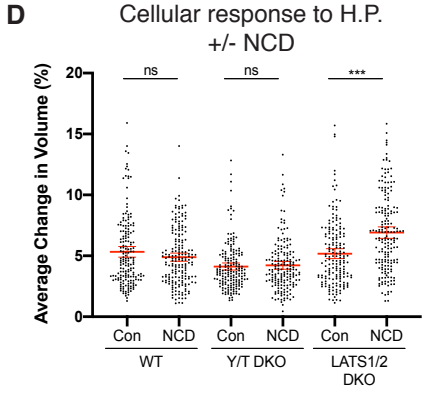
D
Cellular response to H.P.
+/- NCD
Average Change in Volume (%)
20
15
10
5
0
ns
***

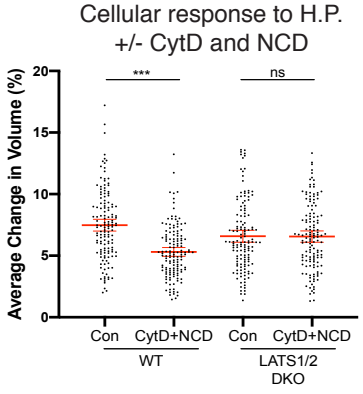
E
Cellular response to H.P.
+/- CytD and NCD
Average Change in Volume (%)
***
ns
Con
CytD+NCD
WT
LATS1/2
DKO

Figure 5

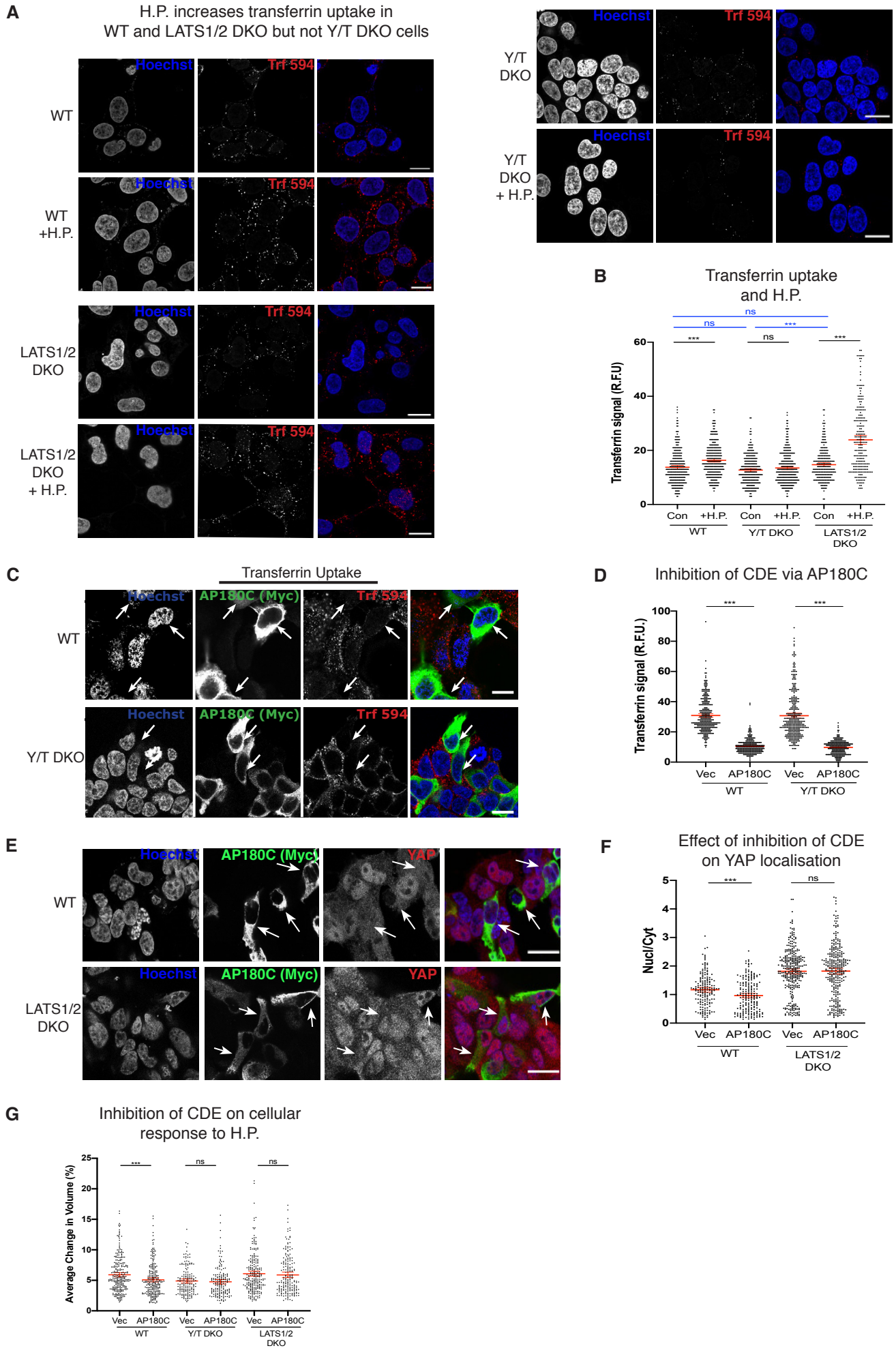
A
H.P. increases transferrin uptake in
WT and LATS1/2 DKO but not Y/T DKO cells
WT
WT +H.P.
LATS1/2 DKO
LATS1/2 DKO + H.P.
Y/T DKO
Y/T DKO + H.P.
Hoechst
Trf 594
B
Transferrin uptake and H.P.
Transferrin signal (R.F.U)
Con
+H.P.
WT
Y/T DKO
LATS1/2 DKO
C
Transferrin Uptake
AP180C (Myc)
D
Inhibition of CDE via AP180C
Transferrin signal (R.F.U.)
Vec
AP180C
E
YAP
F
Effect of inhibition of CDE on YAP localisation
Nucl/Cyt
G
Inhibition of CDE on cellular response to H.P.
Average Change in Volume (%)

EV1

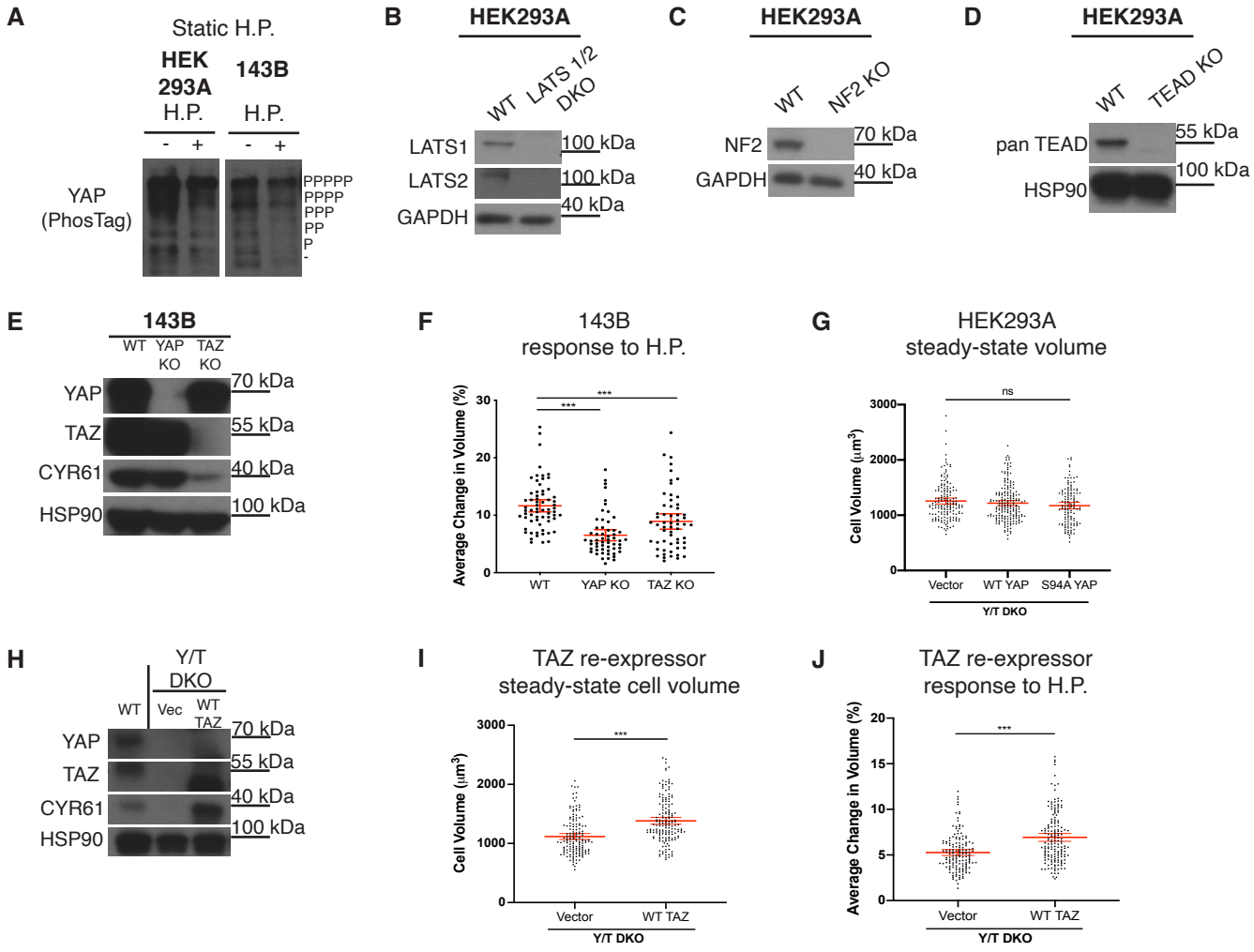
A
Static H.P.
HEK 293A H.P.
143B H.P.
- + - +
YAP (PhosTag)
PPPPP
PPPP
PPP
PP
P
-
B
HEK293A
WT
LATS 1/2 DKO
LATS1
LATS2
GAPDH
100 kDa
100 kDa
40 kDa
C
HEK293A
WT
NF2 KO
NF2
GAPDH
70 kDa
40 kDa
D
HEK293A
WT
TEAD KO
pan TEAD
HSP90
55 kDa
100 kDa
E
143B
WT
YAP KO
TAZ KO
YAP
TAZ
CYR61
HSP90
70 kDa
55 kDa
40 kDa
100 kDa
F
143B response to H.P.
Average Change in Volume (%)
WT
YAP KO
TAZ KO
G
HEK293A steady-state volume
Cell Volume (μm³)
ns
Vector
WT YAP
S94A YAP
Y/T DKO
H
Y/T DKO
WT
Vec
WT TAZ
YAP
TAZ
CYR61
HSP90
70 kDa
55 kDa
40 kDa
100 kDa
I
TAZ re-expressor steady-state cell volume
Cell Volume (μm³)
Vector
WT TAZ
Y/T DKO
J
TAZ re-expressor response to H.P.
Average Change in Volume (%)
Vector
WT TAZ
Y/T DKO

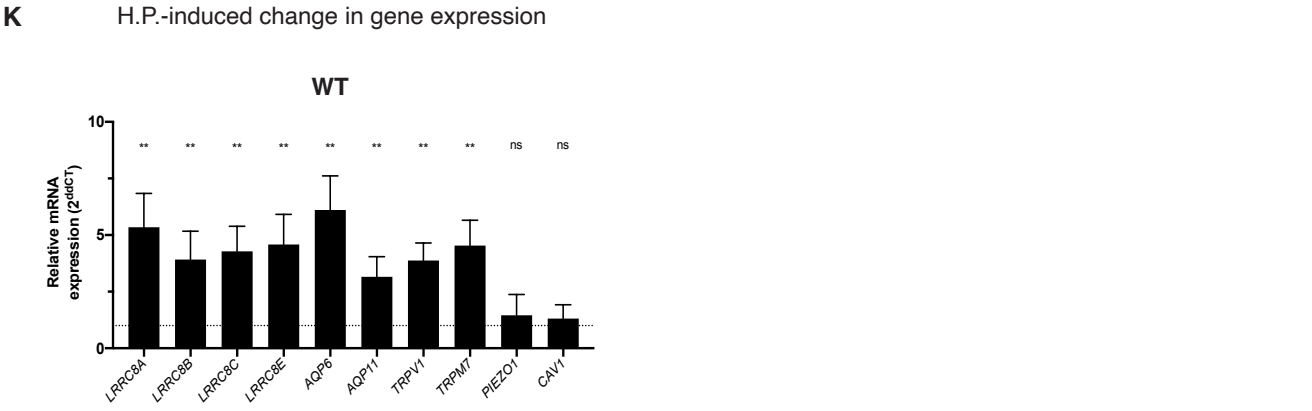
K
H.P.-induced change in gene expression
WT
Relative mRNA expression (2^ddCT)
LRRC8A
LRRC8B
LRRC8C
LRRC8E
AQP6
AQP11
TRPV1
TRPM7
PIEZO1
CAV1

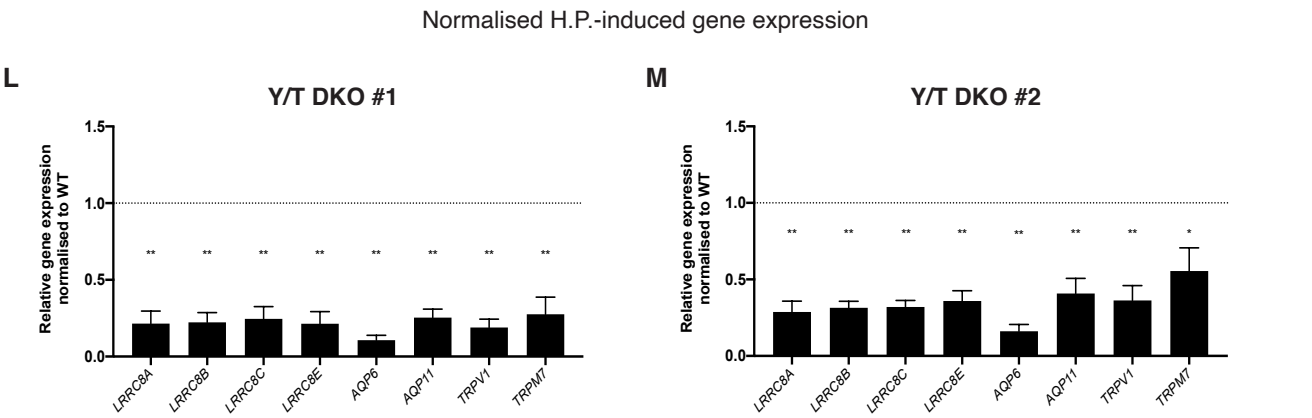
Normalised H.P.-induced gene expression
L
Y/T DKO #1
Relative gene expression normalised to WT
M
Y/T DKO #2
Relative gene expression normalised to WT
LRRC8A
LRRC8B
LRRC8C
LRRC8E
AQP6
AQP11
TRPV1
TRPM7

EV2

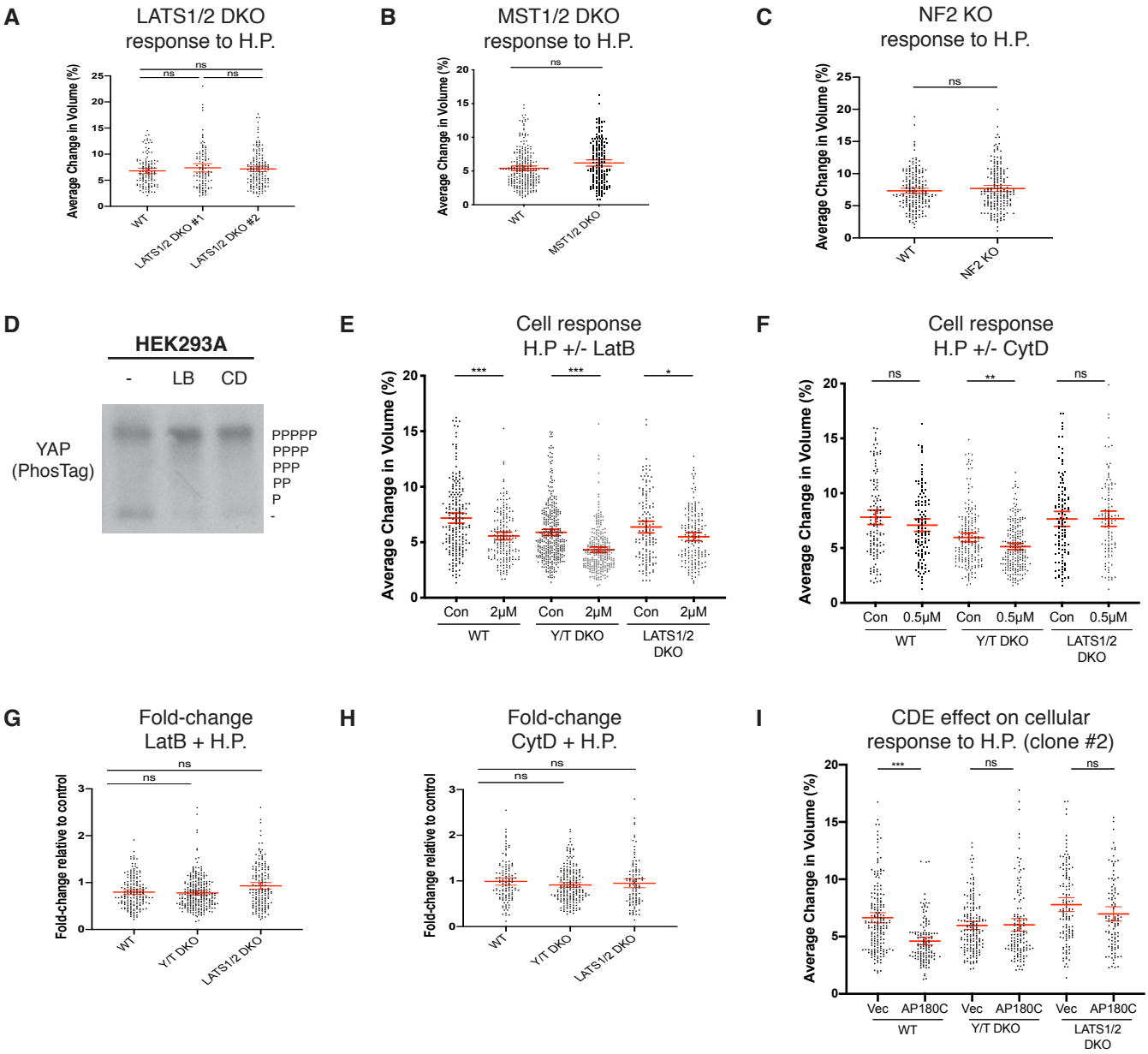
A
LATS1/2 DKO
response to H.P.
Average Change in Volume (%)
ns
WT
LATS1/2 DKO #1
LATS1/2 DKO #2
B
MST1/2 DKO
response to H.P.
MST1/2 DKO
C
NF2 KO
response to H.P.
NF2 KO
D
HEK293A
- LB CD
YAP
(PhosTag)
PPPPP
PPPP
PPP
PP
P
-
E
Cell response
H.P +/- LatB
***
*
Con
2μM
WT
Y/T DKO
LATS1/2
DKO
F
Cell response
H.P +/- CytD
**
0.5μM
G
Fold-change
LatB + H.P.
Fold-change relative to control
H
Fold-change
CytD + H.P.
I
CDE effect on cellular
response to H.P. (clone #2)
Vec
AP180C

EV3

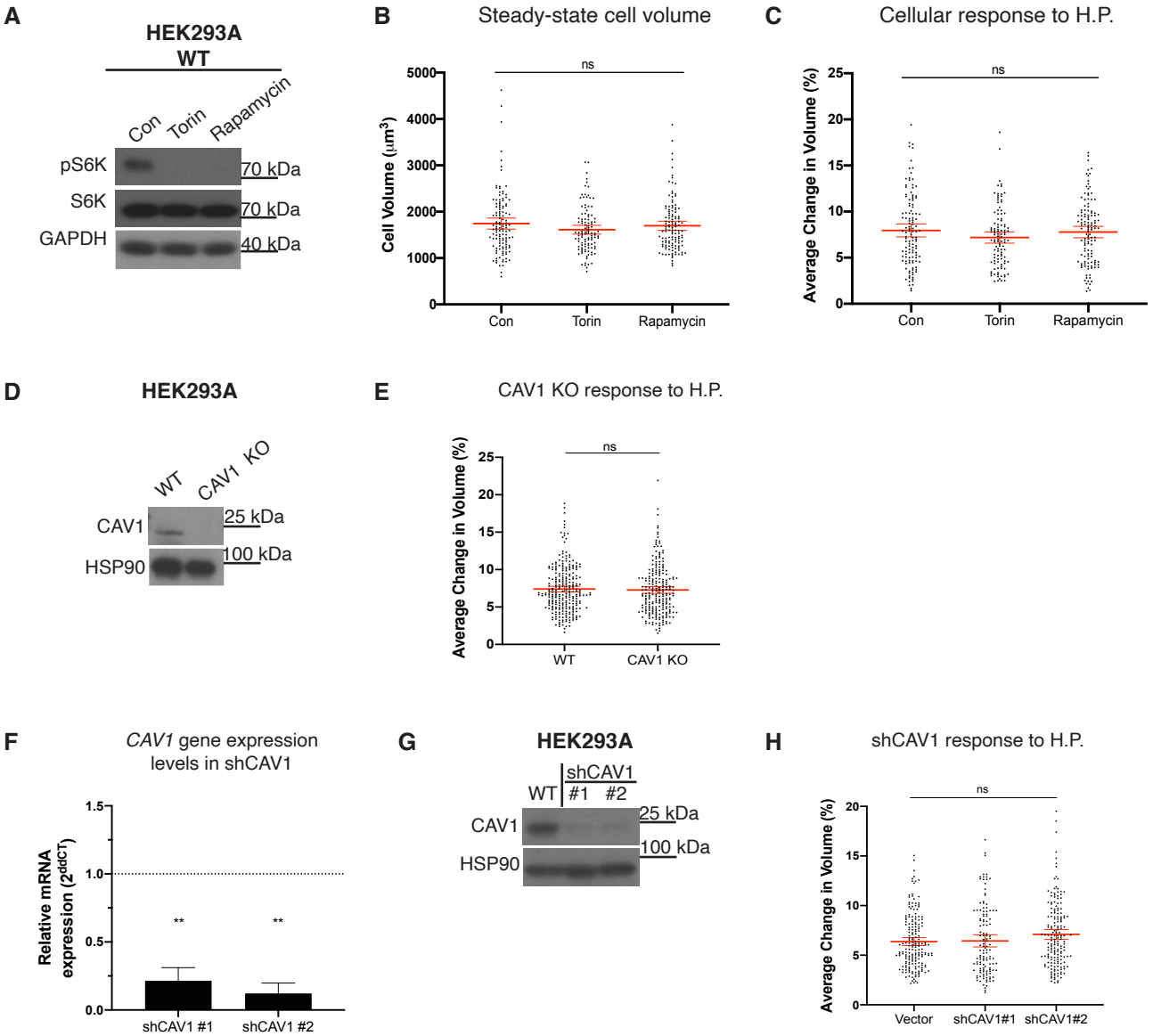
A
HEK293A
WT
Con
Torin
Rapamycin
pS6K
S6K
GAPDH
70 kDa
70 kDa
40 kDa
B
Steady-state cell volume
ns
Cell Volume (μm³)
5000
4000
3000
2000
1000
0
Con
Torin
Rapamycin
C
Cellular response to H.P.
ns
Average Change in Volume (%)
25
20
15
10
5
0
Con
Torin
Rapamycin
D
HEK293A
WT
CAV1 KO
CAV1
HSP90
25 kDa
100 kDa
E
CAV1 KO response to H.P.
ns
Average Change in Volume (%)
25
20
15
10
5
0
WT
CAV1 KO
F
CAV1 gene expression levels in shCAV1
Relative mRNA expression (2ddCT)
1.5
1.0
0.5
0.0
**
**
shCAV1 #1
shCAV1 #2
G
HEK293A
WT
shCAV1 #1
shCAV1 #2
CAV1
HSP90
25 kDa
100 kDa
H
shCAV1 response to H.P.
ns
Average Change in Volume (%)
20
15
10
5
0
Vector
shCAV1#1
shCAV1#2

EV4

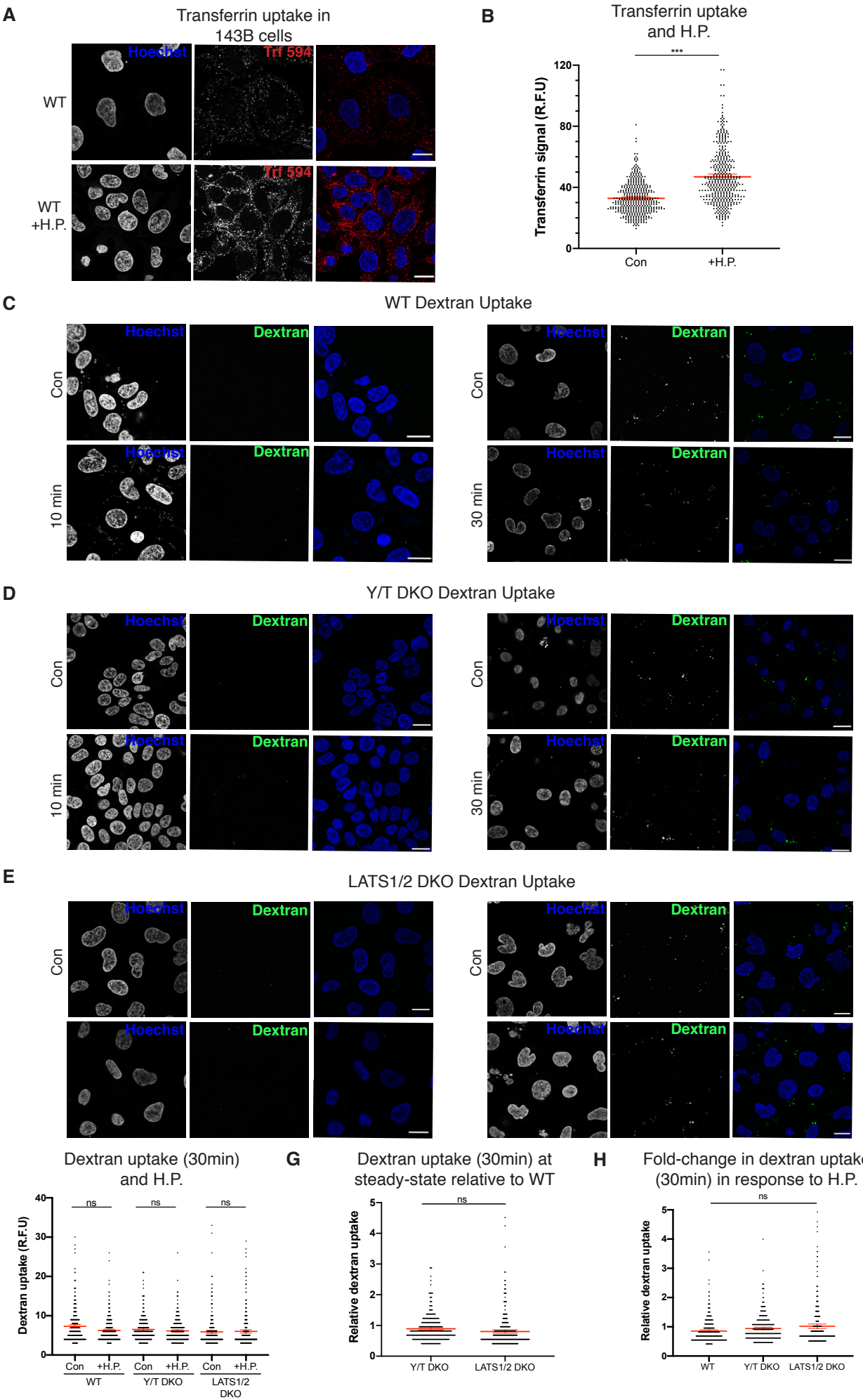
A
Transferrin uptake in 143B cells
Hoechst
Trf 594
WT
WT +H.P.
B
Transferrin uptake and H.P.
***
Transferrin signal (R.F.U)
120
80
40
0
Con
+H.P.
C
WT Dextran Uptake
Hoechst
Dextran
Con
10 min
30 min
D
Y/T DKO Dextran Uptake
E
LATS1/2 DKO Dextran Uptake
F
Dextran uptake (30min) and H.P.
ns
Dextran uptake (R.F.U)
40
30
20
10
0
Con
+H.P.
WT
Y/T DKO
LATS1/2 DKO
G
Dextran uptake (30min) at steady-state relative to WT
Relative dextran uptake
5
4
3
2
1
0
Y/T DKO
LATS1/2 DKO
H
Fold-change in dextran uptake (30min) in response to H.P.
Relative dextran uptake
WT
Y/T DKO
LATS1/2 DKO

EV5

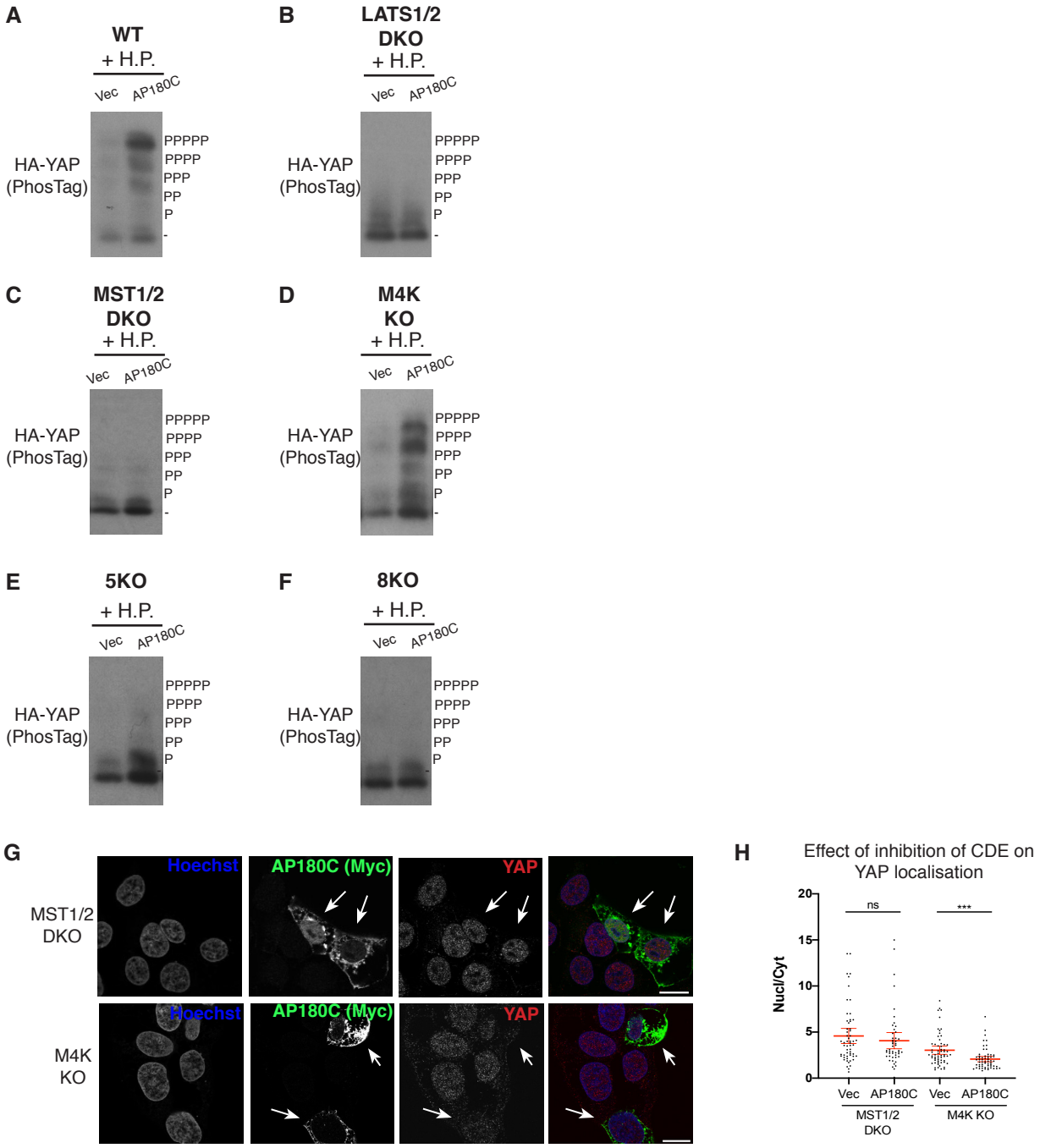
A
WT
+ H.P.
Vec
AP180C
HA-YAP
(PhosTag)
PPPPP
PPPP
PPP
PP
P
-
B
LATS1/2
DKO
+ H.P.
C
MST1/2
DKO
+ H.P.
D
M4K
KO
+ H.P.
E
5KO
+ H.P.
F
8KO
+ H.P.
G
MST1/2
DKO
M4K
KO
Hoechst
AP180C (Myc)
YAP
H
Effect of inhibition of CDE on
YAP localisation
Nucl/Cyt
ns
***
MST1/2
DKO
M4K KO